Bulletin of the Seismological Society of America, 90, 2, pp. 425–449, April 2000

Earthquake Locations in the Inner Continental Borderland, Offshore Southern California

by Luciana Astiz and Peter M. Shearer

Abstract The inner Continental Borderland region, offshore southern California, is tectonically active and contains several faults that are potential seismic hazards to nearby cities. However, fault geometries in this complex region are often poorly constrained due to a lack of surface observations and uncertainties in earthquake locations and focal mechanisms. To improve the accuracy of event locations in this area, we apply new location methods to 4312 offshore seismic events that occurred between 1981 and 1997 in seven different regions within the Borderland. The regions are defined by either temporal or spatial clustering of seismic activity in the Southern California Seismic Network (SCSN) catalog. Obtaining accurate locations for these events is difficult, due to the lack of nearby stations, the limited azimuthal coverage, and uncertainties in the velocity structure for this area. Our location procedure is based on the L-1 norm, grid search, waveform cross-correlation method of Shearer (1997), except that we use a nearest neighbor approach (Astiz *et al.*, 2000) to identify suitable event pairs for waveform cross-correlation and we explore the effect of different velocity models on the locations and associated station terms. In general, our relocated events have small estimated relative location errors and the events are more clustered than the SCSN catalog locations. A quarry on the south tip of Catalina Island provides a test of our location accuracy and suggests that, under ideal conditions, offshore events can be located to within 1 to 2 km of their true locations. Our final locations for most clusters are well correlated with known local tectonic features. We relate the 1981 Santa Barbara Island ($M_L = 5.3$) earthquake with the Santa Cruz fault, the 13 July 1986 Oceanside ($M_L = 5.3$) sequence with the San Diego Trough fault zone, and events near San Clemente Island with the known trace of the San Clemente fault zone. Over 3000 of the offshore events during this time period are associated with the 1986 Oceanside earthquake and its extended aftershock sequence. Our locations define a northeast-dipping fault plane for the Oceanside sequence, but in cross-section the events are scattered over a broad zone (about 4-km thick). This could either be an expression of fault complexity or location errors due to unaccounted for variations in the velocity structure. Events that occur near Coronado Bank in the SCSN catalog are relocated closer to the San Diego coast and suggest a shallow-angle, northeast-dipping fault plane at 10 to 15 km depth.

Introduction

The Continental Borderland is an offshore geomorphic region extending from Point Conception in southern California to the Vizcaíno Peninsula in Baja California, Mexico, that contrasts markedly with the nearly flat 30- to 50-km wide continental shelf off most of the Californias. It is a 250-km-wide zone of bathymetric lows (basins and troughs) and highs (ridges, banks, knolls, and islands) that separate the coast from the abyssal floor of the Pacific Ocean. The Patton Escarpment to the north and the Cedros Deep to the south (Moore, 1969) delineate its western limit. Observed low free-air gravity anomalies occur over basins whereas high free-air gravity anomalies are mostly associated with ridges and knolls (Beyer, 1980). All basin and ridge structures are subparallel to the northwest trending coast and to the relative motion between the Pacific and North American plates, with the exception of the west-trending Santa Barbara Channel and Channel Islands, which are more consistent with the compressional tectonics of the Transverse Ranges (see inset Figure 1). Many investigators have recognized the complex tectonics and geologic history of this region (e.g., Vedder *et*

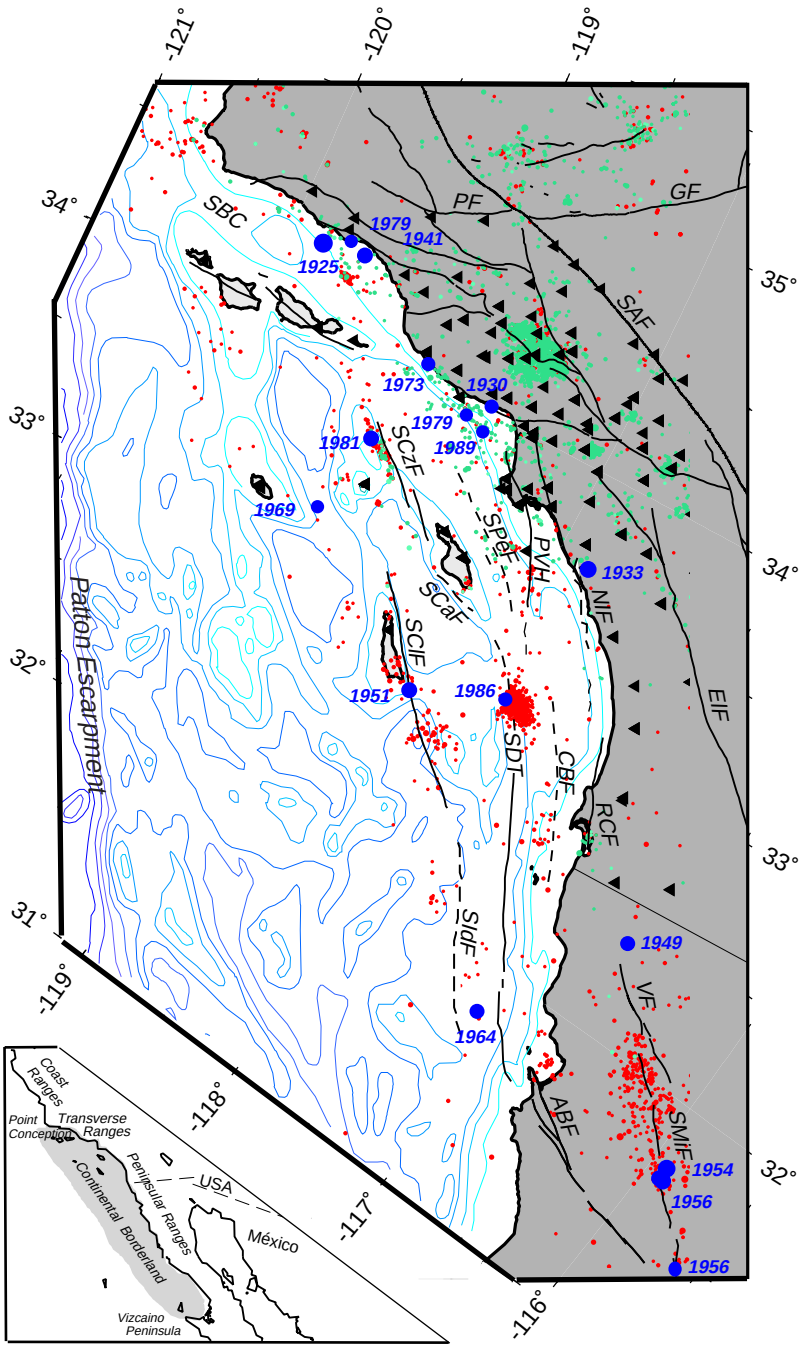

Figure 1. Tectonic map of the Borderland region, offshore southern California, United States, and northern Baja California, Mexico, where mapped and inferred faults are indicated by continuous and dashed lines and bathymetric contours are shown in light gray lines. Dark circles show epicenters of $M_L \geqq 5.0$ events in the Continental Borderland from 1920 to 1997. Light and dark gray dots indicate the epicenters of A + B and C + D event quality locations, respectively, from the SCSN catalog since 1981. Black triangles are station locations used in our locations. Map inset in the lower left shows the extent of the Continental Borderland geologic province. ABF, Agua Blanca Fault; CBF, Coronado Bank Fault Zone; ElF, Elsinore Fault; GF, Garlock Fault; NIF, Newport-Inglewood Fault; PF, Big Pine Fault; PVH, Palos Verdes Hills Fault; RCF, Rose Canyon Fault; SAF, San Andreas Fault; SBC, Santa Barbara Channel; SCaF, Santa Catalina Fault; SClF, San Clemente Fault; SCzF, Santa Cruz Fault; SDT, San Diego Trough Fault; SIdF, San Isidro Fault; SMiF, San Miguel Fault; SPeF, San Pedro Basin Fault Zone; VF, Vallecitos Fault.

al., 1974; Yeats, 1976; Howell and Vedder, 1981; Crouch, 1981; Weldon and Humphreys, 1986; Atwater, 1989; Lonsdale, 1991; Legg, 1991; Crouch and Suppe, 1993; Mann and Gordon, 1996; Hey, 1998; Bohannon and Geist, 1998) and related the steep linear escarpments to faulting (Legg and Ortega, 1978; Clarke *et al.*, 1985; Legg, 1989) which has been invoked to explain different kinematic models (Atwater, 1970; Junger, 1979; Crouch, 1981; Bird and Rosenstock, 1984).

Legg and Kennedy (1979) divide the northwest trending faults in the Continental Borderland into four major subparallel groups. The easternmost fault zone includes the Newport–Inglewood and Rose Canyon faults, passing onshore at San Diego and perhaps connecting with the Vallecitos and San Miguel faults to the south in Baja California (Brune *et al.*, 1979). The second zone is the Palos Verdes Hills–Coronado Bank–Agua Blanca fault that passes onshore alongside Punta Banda near Ensenada, Mexico. To the west is the Santa Cruz–Santa Catalina–San Pedro–San Diego Trough–Bahia Soledad fault trend that passes onshore south of Punta

Banda. The fourth group is the Santa Cruz–San Clemente–San Isidro fault zone. The dramatic seafloor escarpments of the larger banks, ridges, and islands indicate that these faults may have a significant component of dip-slip motion, but displacement of submarine canyons alongside the first three groups of faults indicates right-lateral strike-slip motion consistent with the regional tectonics associated with the San Andreas fault system. Geodetic measurements in this region indicate right-lateral strike-slip motion along the faults east of San Clemente Island, which is moving at a rate of 5.9 ± 1.8 mm/yr in a 38°N ± 20°W direction relative to San Diego; the motion measured further west is insignificant (Larson, 1993). Recent seismicity from the Southern California Seismic Network (SCSN) catalog indicates that tectonic deformation is mainly taking place in the inner Continental Borderland (i.e., east of the Santa Cruz–San Clemente–San Isidro fault zone) and in the Santa Barbara Channel as illustrated in Figure 1.

Seismicity in the Borderland is diffuse even for those events associated with main-shock sequences; this could, however, be mostly an artifact of routine epicentral locations as given by the SCSN catalog, partly due to large lateral heterogeneities in the velocity models as suggested by the complex geology and bathymetric extremes in the region (Vedder, *et al.*, 1974; Legg, 1985, 1989), and also to the asymmetrical distribution of stations that record these events. Locating earthquakes under these conditions is difficult, and is especially challenging for those events occurring the furthest offshore. It is not surprising the vast majority of the SCSN catalog locations for offshore southern California events are assigned the low-quality "C" and "D" rankings; most catalog depths for these events are constrained at 6 km since the station distribution does not allow for accurate depth estimates in the standard location procedure. Although the accuracy of the offshore earthquake locations is limited, the seismicity does appear to align near known tectonic features.

The damaging 1933 Long Beach (M_L = 6.3) earthquake ruptured a 30-km long segment of the Newport–Inglewood fault (Richter, 1958) with pure right-lateral strike-slip motion on a N40°W plane as indicated by the focal mechanism derived from teleseismic waveforms (Woodward-Clyde Consultants, 1979). Hauksson (1987) studied in detail the seismotectonics of the Newport-Inglewood fault zone in the Los Angeles area. This fault may connect to the Rose Canyon fault in San Diego (Heaton and Jones, 1989), and possibly to the Vallecitos–San Miguel faults in Baja California, where two large earthquakes occurred in 1954 (M_L = 6.0, 6.3) and four more during 1956 (M_L = 6.8, 6.1, 6.3, and 6.4), indicating right-lateral strike-slip motion along the San Miguel fault (Brune *et al.*, 1979; Leeds, 1979). Moderate (M_L = 5 to 6) earthquakes in the inner Continental Borderland region are associated with the regional tectonics dominated by the San Andreas fault (e.g., Weldon and Humphreys, 1986). Many of these events, however, have significant dip-slip components of motion, including the largest recorded offshore event, the San Clemente Island (M_L = 5.9) earthquake of 26 December 1951 (Richter, 1958, p. 535; Allen *et al.*, 1960).

Other large events occurring near right-lateral strike-slip northwest trending faults include the 1981 Santa Barbara Island (M_L = 5.3) earthquakes along the Santa Cruz–Santa Catalina fault (Corbett, 1984) and the 1964 (M_L = 5.6) Ensenada event, which may be associated with the Maximinos or San Isidro faults (Cruces and Rebollar, 1991). Smaller events generally have either a right-lateral strike-slip mechanism like the 1969 Santa Cruz Basin (M_L = 5.1) earthquake (Legg, 1980) or a thrust mechanism like the 1986 Oceanside (M_L = 5.3) earthquake occurring at the northern end of the San Diego Trough fault region (Hauksson and Jones, 1988; Pacheco and Nábêleck, 1988). On the other hand, seismicity associated with the Santa Barbara Channel reflects the compressional tectonics of the Transverse Ranges, with seismicity occurring both in swarms such as the 1968 (Sylvester *et al.*, 1970) and 1978 (Whitcomb *et al.*, 1979) sequences and in mainshock sequences such as those following the 1925 Santa Barbara (M_L = 6.3), the 1941 Carpenteria (M_L = 5.9), and 1979 Santa Barbara (M_L = 5.1) events (Corbett and Johnson, 1982). These events broke east-striking north-dipping thrust faults in agreement with the mapped geology of the region (Vedder *et al.*, 1974; Lee *et al.*, 1979). Further west, the 1930 Santa Monica (M_L = 5.2) (Gutenberg *et al.*, 1932), the 1973 Point Magu (M_L = 6.0) (Stierman and Ellsworth, 1976) and the 1979 and 1989 Malibu (M_L = 5.0, 5.0) earthquakes (Hauksson and Saldivar, 1986, 1989; Hauksson, 1990) also took place on east-striking north-dipping thrust faults. Epicenters for the events are indicated by dark circles in Figure 1.

Understanding the fault geometries and tectonics of the Borderland region is important for assessing the seismic hazard that offshore faults may pose to southern California. Several researchers have used master event and joint hypocenter techniques to locate events in parts the Continental Borderland region (e.g., Corbett and Johnson, 1982; Corbett, 1984; Saldivar, 1987; Hauksson and Saldivar, 1989; Hauksson, 1990). Here we adopt a systematic approach to locating events in this region using the L1-norm method developed by Shearer (1997). To obtain the best possible constraints on the event locations, we obtain additional *P*- and *S*-arrival times using waveform cross-correlation among adjacent events. Since there is some uncertainty regarding the best velocity model to use in the Borderland, we examine seven different subregions and explore the effects on the locations of different models and range limits on the stations. Finally, we relate the results to the known bathymetry and tectonics in each area.

Location Method

We use the grid-search, L1-norm location procedure described by Shearer (1997) and Astiz *et al.* (2000). The method has a number of features to improve location accu-

racy, including: (1) L1-norm misfit criteria, (2) adjusted travel time picks based on waveform cross-correlation, and (3) custom station terms for each cluster of events. The use of the L1-norm minimizes the effect of outliers in the arrival-time residuals compared to more conventional least-squares methods. In southern California we have found that L1-norm locations show much less scatter, particularly in depth, than L2-norm locations (Shearer, 1997, 1998; Astiz *et al.*, 2000). Records of nearby events are often sufficiently similar that waveform cross-correlation can be used to greatly improve the timing accuracy of arrivals and yield more precise locations (e.g., Poupinet *et al.*, 1984; Fremont and Malone, 1987; Got *et al.*, 1994; Nadeau *et al.*, 1995; Haase *et al.*, 1995; Dodge *et al.*, 1996, Gillard *et al.*, 1996; Rubin *et al.*, 1999). Here we perform waveform cross-correlation among nearby events selected using the natural neighbor approach of Astiz *et al.* (2000). Station terms are used to account for the effect of three-dimensional-velocity structure outside the source regions (e.g., Frohlich, 1979; Pujol, 1988, 1995); this provides relative location errors comparable to those achieved with master event methods (e.g., Evernden, 1969; Jordan and Sverdrup, 1981). Here we solve for a separate set of station terms for each of the offshore seismicity clusters; our final locations are based only upon those stations with associated station terms. These station terms improve the relative location accuracy among events within the cluster but do not generally affect the absolute location accuracy of the entire cluster. To obtain the best possible absolute location accuracy for the offshore events, we attempt to identify the most appropriate one-dimensional velocity model for each of the clusters.

Velocity Models

SCSN catalog locations are based on the Hadley and Kanamori (1977) one-dimensional velocity model, which has a crustal depth of 32 km and mantle *Pn* velocity of 7.8 km/sec. This model is a reasonable approximation to the true velocity structure throughout much of southern California, but is not appropriate for locating offshore earthquakes due to the much thinner crust in this region. Results from refraction experiments in offshore southern California were compiled by Shor *et al.* (1976), who concluded that velocity profiles can change rapidly within the Borderland region, but that the crust thins from 24 km depth under the Catalina Basin to about 16 km at the top, and 10 km at the foot, of the Patton escarpment (see Figure 1). Corbett (1984) determined simple one-dimensional velocity models for the inner Continental Borderland region from quarry blasts recorded by the SCSN and estimated the crustal depth at 22 km northwest of Catalina Island and 19 km to the west and south, with *Pn* velocities of 7.8 km/sec. Magistrale *et al.* (1992) from inversion of *P* arrivals to the SCSN and using the Corbett results as starting models, obtained a Moho depth of 26 km to the northwest of Catalina Island and 20 km to the southwest, with a mantle *Pn* velocity near 8 km/sec.

We consider several smooth one-dimensional velocity models (Fig. 2) that incorporate the main features found in the Continental Borderland from these studies and from models resulting from earthquake location efforts in the Santa Monica Bay (Hauksson and Saldivar, 1989) and Oceanside regions (Hauksson and Jones, 1988). Our base model, *oce1*, has three layers with *P* velocity of 3.3 km/sec at 0 km, increasing to 6.0 km/sec at 6-km depth and to 6.5 km/sec at 24-km depth, where the mantle velocity jumps to 7.8 km/sec. The velocity at the surface is 2.6 km/sec and 4.0 km/sec for models *oce2* and *oce3*, respectively, which have the same velocity profile as *oce1* at depth. The shallower velocity profile of *oce1* is shared by models *oce4* and *oce5*, but the Moho depth changes to 22- and 26-km depth, respectively. A scaled version of the *P* model is used as a reference *S*-velocity model, assuming a Poisson's ratio of 0.25.

An advantage of using smooth velocity models is that we can generate travel-time curves that are easily interpolated in range and depth without generating artifacts due to edge effects. From these models, we compute *P* and *S* travel-time tables from each station to a three-dimensional grid that surrounds the events. Since the regions in Figure 2 are relatively large, the grid spacing for most of the regions is 2 km in the horizontal direction and 1 km in depth, with the exception of Santa Catalina, where we take 1-km-grid spacing in all directions. The travel-time array can be large depending on the size of the grid and the number of stations (e.g., a 25 by 25 by 25 grid and 50 stations yields 1,562,500 *P* and *S* travel times) but needs to be calculated only once and can then be used to locate all the events within the volume. For each event, the observed *P* and *S* travel-time picks are compared to those predicted at each grid point, and the best-fitting grid point is located. The location is then further refined by examining a finer grid obtained by interpolation between adjacent grid points. All locations shown in this article are computed to a nominal resolution of 15 m.

Due to strong tradeoffs between the velocity model and the event depths and origin times for these offshore events, it is not practical to invert the data uniquely for a single best-fitting velocity model. In addition, it is likely that lateral velocity variations are present across the region that would limit the applicability of a single one-dimensional-velocity model for earthquake locations. Our approach is to separately examine each local region of interest and explore the effect on the locations of a suite of models (see Figure 2) that are similar to those previously obtained for the Borderland region from refraction profiling and analysis of calibration shots (e.g., Shor *et al.*, 1976; Corbett, 1984). From these results, we select our final model for each region based on the following criteria: (1) the locations should cluster reasonably in depth and not clump at the top or bottom of their allowed depth interval, (2) the locations should not change significantly when a different range cutoff is applied to the station distribution, and (3) the station terms computed in the location procedure should correlate reasonably with local geology and not exhibit a strong range dependence (which

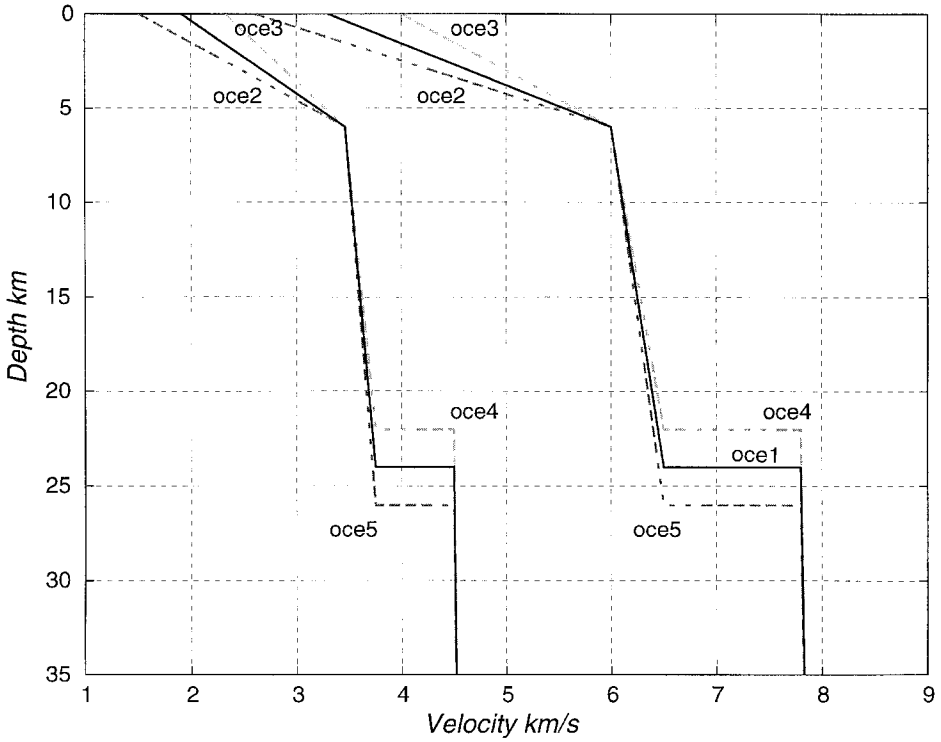

Figure 2. *P*- and *S*-wave-velocity models used to locate the Borderland events. The solid line defines the *oce1* model. The *oce2* and *oce3* models differ in the upper crust but coincide with *oce1* near the Moho. The *oce4* and *oce5* models have different Moho depths but coincide with *oce1* in the upper crust.

would suggest a problem with the one-dimensional-velocity model).

Waveform Cross-Correlation with Natural Neighbors

In the case of similar event pairs, waveform cross-correlation can be used both to improve the consistency of the original arrival-time picks and to obtain picks for traces that were originally unpicked (Shearer, 1998; Astiz *et al.*, 2000). SCSN waveform data suitable for cross-correlation are easily available from the SCEC Data Center, and we extracted all available traces for the offshore events. Due to sampling rate fluctuations in the SCSN stations since 1981, we resampled the waveforms to a uniform 100 Hz, and since waveform cross-correlation is more stable at lower frequencies, we also applied a 10-Hz low-pass filter to the over 295,000 traces recorded by southern California stations located within 200 km of the events. Waveform cross-correlation produces accurate differential times only if the event waveforms are significantly correlated. This requires similarity in both the event locations and focal mechanisms, as might occur for nearby events on the same fault. Waveforms of closely located events have been observed to have high correlation coefficients at individual stations (Pechmann and Kanamori, 1982; Pechmann and Thorbjarnardottir, 1990; Mezcua and Rueda, 1994; Slad and Aster, 1995).

For small clusters of events, it is easy to cross-correlate every event pair, but for larger numbers of events this becomes computationally impractical. To limit the computation time for regions with more than 150 events (Table 1), we only determine cross-correlation functions among a particular event and 100 of its nearest neighbors (Sambridge *et al.*, 1995; Astiz *et al.*, 2000). The cross-correlation procedure is illustrated in Figure 3 for a pair of two similar earthquakes from the Oceanside sequence, a $M_L = 2.4$ event (January 6, 1985, 1217 UT) and a $M_L = 2.9$ event (August 3, 1986, 1902 UT). Note that about half of the pairs show a well-defined maximum that can be used as a measure of the differential time between the traces. We use different window lengths for events in each region to maximize the cor-

Table 1
Cross-Correlation and "Tree" Definition Parameters

Region	Nev	P window (sec) beg., end, length	S window (sec) beg., end, length	min. Nev for tree	min. X-corr.
SBI	604	−1.00, 1.00 (2.0)	−1.00, 2.00 (3.0)	10	0.47
SCA	21	−1.75, 0.75 (2.5)	−0.75, 2.25 (3.0)	6	0.45
OCS	3215	−1.25, 0.75 (2.0)	−2.00, 1.00 (3.0)	20	0.55
CBK	104	−1.75, 0.75 (2.5)	−0.75, 2.25 (3.0)	6	0.45
SCLN	56	−1.50, 1.50 (3.0)	−2.00, 2.00 (4.0)	6	0.45
SCL	81	−1.50, 1.50 (3.0)	−2.00, 2.00 (4.0)	6	0.45
SCLS	219	−2.00, 1.00 (3.0)	−2.00, 2.00 (4.0)	6	0.45

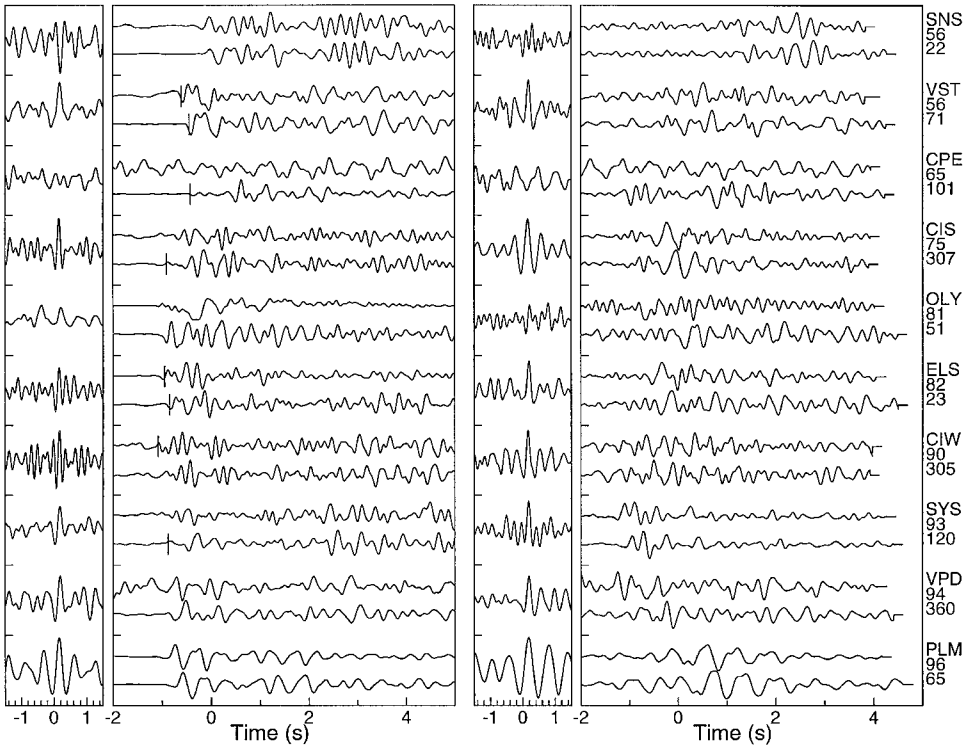

Figure 3. Waveform cross-correlation applied to a pair of similar earthquakes from the Oceanside sequence, an $M_L = 2.4$ event (January 6, 1985, 1217 UT) on the left and an $M_L = 2.9$ event (August 3, 1986, 1902 UT) on the right. The larger boxes show the *P* and *S* waves recorded at the ten stations listed to the right; the distance in km and azimuth to each station are also indicated. The smaller boxes show the cross-correlation functions computed from these data using 2- and 3-sec windows around the *P* and *S* waves, respectively, with maximum time shifts of $\pm$ 1.5 sec. The traces have been low-pass filtered at 10 Hz. Small vertical lines show the SCSN operator picks (when available). Note that about half of the pairs show a well-defined maximum that can be used as a measure of the differential time between the traces.

relation coefficients between the events. *P*-wave windows ranged between 2 and 3 sec and *S*-wave windows from 3 to 4 sec-long; the maximum allowed time shift between the two waveforms was ± 1.5 sec.

Event clusters that are connected by at least one combination of differential times for a given threshold correlation coefficient are termed "trees" (Aster and Scott, 1993). We varied the minimum number of events and threshold correlation coefficient required for events to form trees among the regions, since the number of events (*Nev*) and the amount of clustering between the events varied considerably. We then combined these differential times with the existing picks to solve for a new set of adjusted picks as described in detail by Shearer (1997). For this procedure we only consider event pairs with an average correlation coefficient for *P* and *S* waves of 0.5 or greater and use only those individual waveform pairs that have a correlation coefficient of 0.7 or greater. Table 1 lists the parameters used in the cross-correlation and "tree" definitions for each of the regions in this study.

Location Uncertainties and Errors

We estimate location errors using a bootstrap approach in which random perturbations are added to the travel times of each event to represent picking errors (Billings *et al.*, 1994; Shearer, 1997). The event is then relocated many separate times to obtain an estimate of the probable scatter in the locations due to uncertainties in the picks. This technique has the advantage of fully including all of the nonlinearities in the problem and also accounts for the fact that some stations and ray paths are much more important than others in constraining the location. For all event groups in the inner Borderland region, the horizontal and vertical errors (*herr* and *zerr*, respectively) were reduced when additional picks were included in the locations. Note that the location errors are not absolute but relative among the events within a group. For most regions offshore *herr* are less than *zerr*, but the median error values for our best locations can range by a factor of ten or more between regions. For example, median error estimates for the Santa Catalina Island cluster are about 60 m, whereas errors for the Coronado Bank regions

are 600 m and those near San Clemente Island range from 1 to 2 km.

Inner Borderland Earthquake Locations

Several researchers have used master event and joint hypocenter techniques to locate events in the Continental Borderland region (e.g., Corbett and Johnson, 1982; Corbett, 1984; Saldivar, 1987; Hauksson and Saldivar, 1989; Hauksson, 1990). We focus on locating events occurring from 1981 to 1997 (the years for which SCSN waveform data are available) within offshore southern California in an area south of the Santa Barbara Channel, north of the international border and west of the Santa Monica Bay and San Pedro Basin (Fig. 4). We locate 4312 events within the seven regions shown in Figure 4: Catalina Island (SCA), Santa Barbara Island (SBI), Oceanside (OCS), Coronado Bank (CBK), and further west near San Clemente Island (SCLN, SCL, SCLS).

Santa Catalina Island Cluster (SCA)

Because these events appear to be mostly explosions from a quarry on the south tip of Santa Catalina Island, this cluster provides a good test of our ability to accurately locate offshore events. There are 21 events within the SCA box (33.25° to 33.35°N, 118.35° to 118.25°W) in the SCSN catalog between 1981 and 1997. Only three events are actually classified as quarry blasts, presumably from the quarry located at the southern end of Santa Catalina Island at 33.3176°N, 118.3053°W (E. Hauksson, personal communication). However, seismograms from the 21 events are very similar, suggesting that almost all of the other events are also quarry blasts. Figure 5 shows waveforms of 16 of these events recorded at station CPE, located about 121 km to the

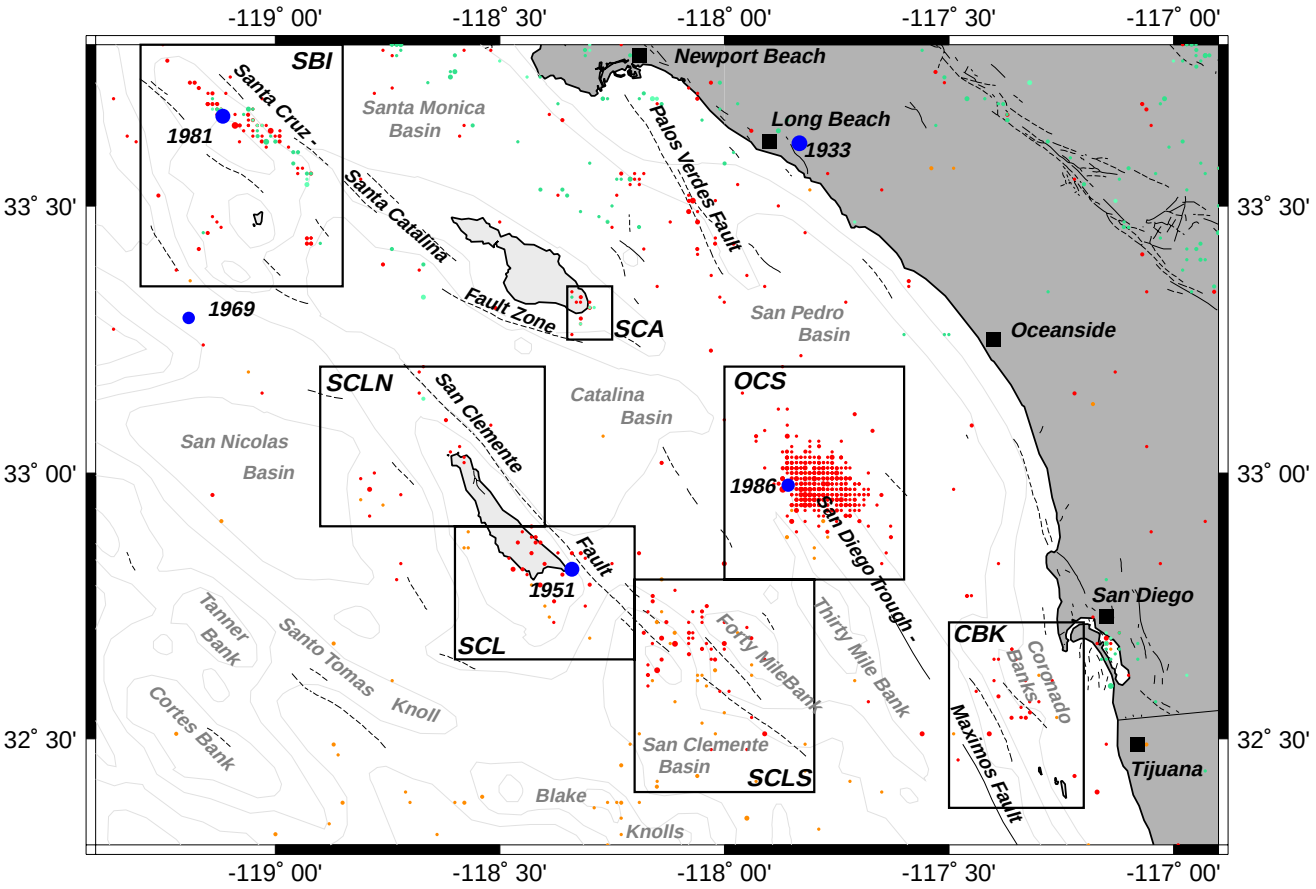

Figure 4. Map of the inner Continental Borderland, offshore southern California, showing the regions for which we located events in this study. Mapped and inferred faults are indicated by continuous and dashed lines and bathymetric contours are shown in light gray lines. Squares indicate the location of population centers. Dark circles show the location of $M_L \geqq 5.0$ events in the region between 1920 and 1997. Light (A and B quality) and dark (C and D quality) gray dots are event locations from the SCSN catalog from 1981 to 1997. Dashed boxes enclose the earthquakes that we located within the following regions: Santa Barbara Island (SBI), Santa Catalina Island (SCA), Oceanside (OCS), Coronado Bank (CBK), and near San Clemente Island (SCLN, SCL, SCLS).

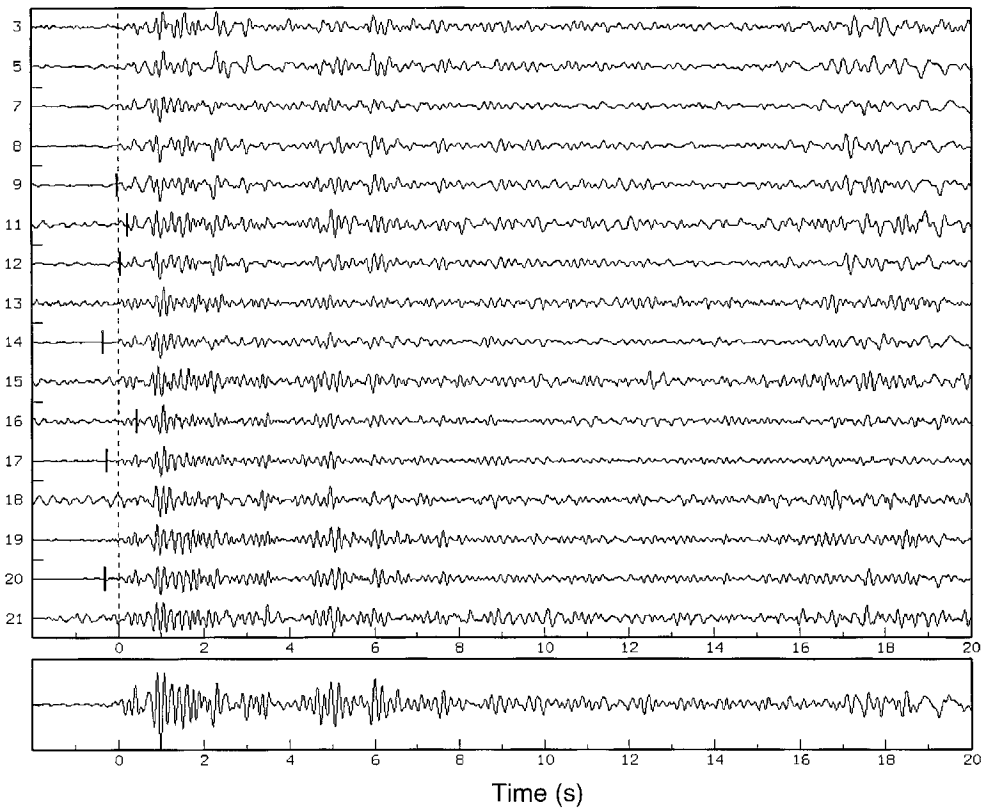

Figure 5. A comparison between the original SCSN analyst *P* picks for a "tree" of 16 Santa Catalina Island events recorded by station CPE and adjusted picks provided by an inversion that included differential times obtained with waveform cross-correlation. SCSN picks were available for seven of the recordings at this station and are indicated by tic marks. The waveforms are aligned on their adjusted picks, shown by the dashed line. The bottom trace is a stack of all the traces above. The event number is indicated to the left. Events 3, 14, and 20 are listed as quarry blasts. Note the waveform similarity between adjacent events (the event numbers are chronological).

southeast of the events. Note the similarity of all waveforms with those radiated by the known quarry blasts (events 3, 14, and 20), but especially among adjacent events. Similar observations can be made from waveforms recorded at other stations. All events occurred during daylight hours, which is further evidence of their human origin (Agnew, 1990).

We used the waveform similarity among these events to improve the relative timing accuracy of the *P* and *S* arrivals using the method of Shearer (1997). We computed cross-correlation coefficients among all 21 events by windowing around the expected *P*-(-1.75 to 0.75 sec) and *S*-(-0.75, 2.25 sec) arrival times from the initial set of locations, using the travel times generated with the *oce1* velocity model. SCSN picks were available for only 7 of the events. For stations located within 125 km, the SCSN analysts had picked 452 *P* and 23 *S* arrivals for these events. After waveform cross-correlation and inversion for a new set of adjusted picks (see Shearer, 1997), we increased the picks to 576 *P* and 149 *S* arrivals, increasing the number of respective picks by an average of 5 and 6 picks per event.

We located the events using the L1-norm algorithm of Shearer (1997), experimenting with using both the original SCSN picks and the adjusted picks from waveform cross-correlation. We also examined the effect of different station range cutoffs and the *oce1* and *oce4* velocity models (24- and 22-km-thick crust, respectively). The number of SCSN stations recording these events increases from 37 within 110 km, to 63 within 125 km, and to 79 within 140 km from the center of the SCA box. The closest stations are located on the island itself, with station CIS at about 12 km and station CIW at nearly 28 km from most events. Estimated standard errors resulting from our location experiments are summarized in Table 2. Although the median standard errors, *herr* and *zerr*, from both velocity models are similar, the best locations are obtained using the *oce4* velocity model and a range cutoff of 125 km, which yield a cluster that is at about 1.5 km depth and less than 1-km southward of the Santa Catalina Island quarry. Locations using stations out to 140 km tend to be shallower but are located further away from the actual quarry site. Our final preferred locations are for the *oce4* velocity model with a station range cutoff of 125 km and include data from 44 stations (within 125 km) that

have more than 5 picks. The resulting station terms are within ± 0.8 sec and correlate with the surface geology.

The improvement in the locations achieved as more advanced location methods are applied is shown in Figure 6, which compares the original SCSN catalog locations to those obtained from the same picks using the L1-norm, both with and without station terms. The final locations are computed using the L1-norm and station terms applied to adjusted picks derived from waveform cross-correlation. The effect of different station range cutoffs to the final locations is il-

Table 2
Horizontal (*herr*) and Vertical (*zerr*) Errors in km for SCA Events

	SCSN Picks				Adjusted Picks			
	Mean		Median		Mean		Median	
Velocity Model	herr	zerr	herr	zerr	herr	zerr	herr	zerr
*oce1*_110	0.8859	1.4029	0.4815	1.4015				
*oce1*_125	0.8452	1.3416	0.3420	0.6320	0.1443	0.2244	0.0580	0.0970
*oce1*_140	0.5995	0.9499	0.3500	0.7330	0.2755	0.3155	0.0870	0.0810
*oce4*_110	0.7963	1.0939	0.5200	0.9985				
*oce4*_125	0.5864	0.9971	0.3780	0.8490	0.1177	0.1220	0.0610	0.0620
*oce4*_140	0.5919	1.0409	0.4000	0.8110	0.2772	0.2605	0.0870	0.0860

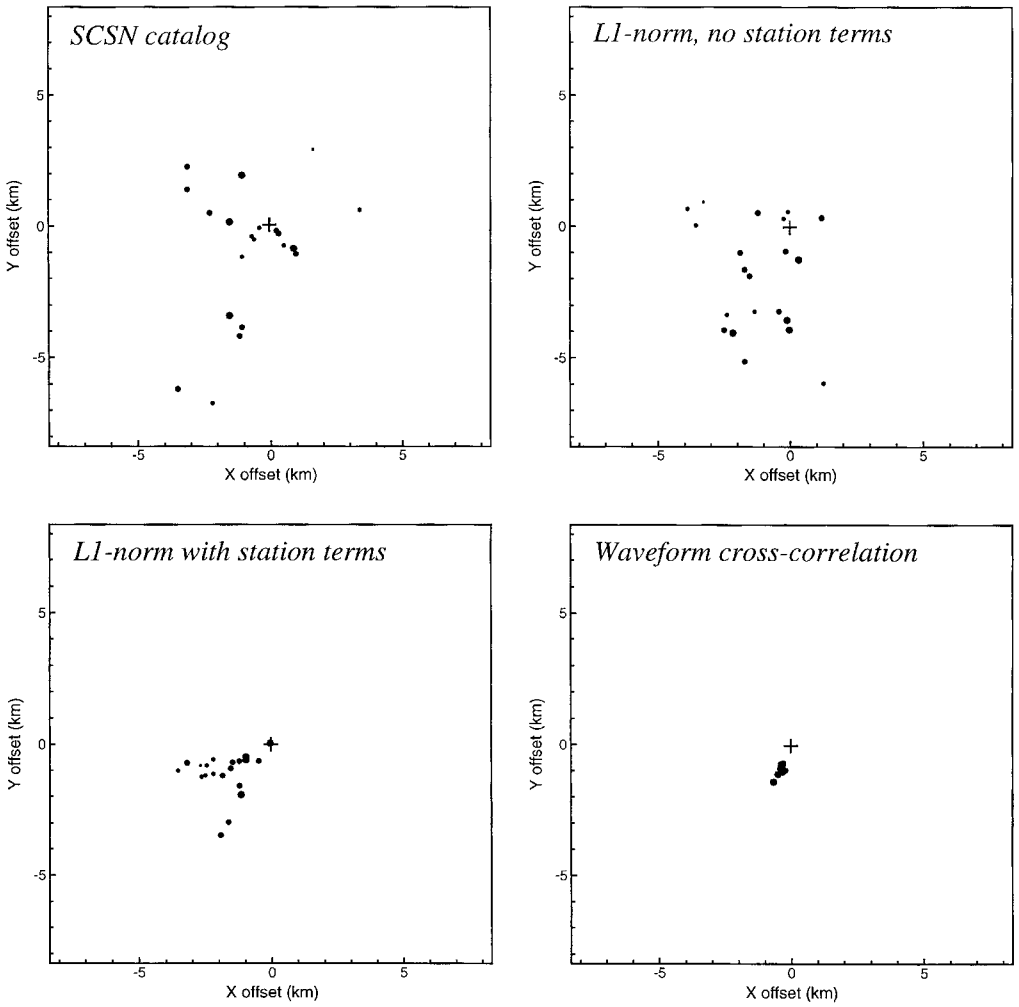

Figure 6. A comparison for Santa Catalina Island events of the original SCSN catalog locations, our locations obtained using the L1-norm (both with and without station terms), and our final locations following waveform cross-correlation. The cross marks the position of the quarry that is the probable true origin of these events.

lustrated in Figure 7 and shows the biasing effects of including stations beyond 125-km range. Finally, Figure 8 compares the locations obtained using the original SCSN picks to those derived from waveform cross-correlation, both in map view and S-N cross-section.

If most of the events in the Santa Catalina cluster are indeed quarry blasts (as the similarity of their waveforms, lack of *S*-wave energy in many of the stations, and their occurrence during daylight hours seem to indicate), this cluster provides a "ground truth" test of our location method. In this case, the absolute horizontal and vertical location errors are about 1 km. In the final locations the event scatter is reduced to an area of about 0.5 km^2, which is much smaller than in our initial locations using the original SCSN picks. The 1-km absolute-location error for this small cluster provides an estimate of the minimum absolute errors that we can expect with the current station distribution for events within offshore southern California. Location errors for other sequences are likely to be larger, due to their reduced waveform similarity compared to this cluster and to their greater distance from nearby island stations.

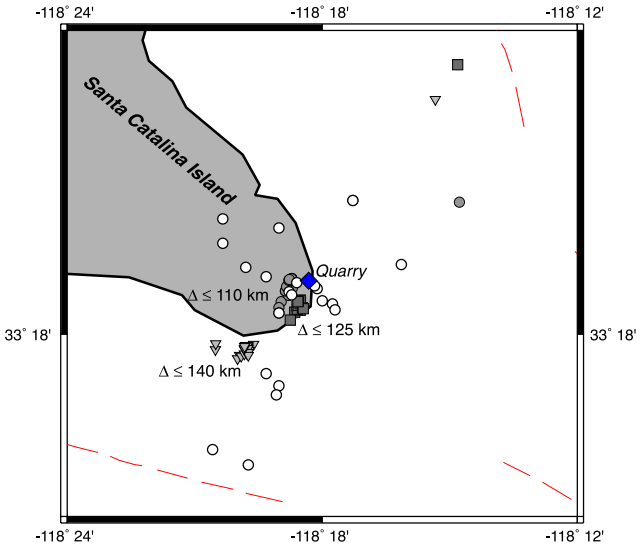

Figure 7. Map showing the southern tip of Santa Catalina Island with inferred faults. The dark diamond shows the location of the Santa Catalina quarry. Open circles indicate the original SCSN catalog locations for the 21 events located within this region. Also shown are our final locations obtained using different values for the maximum station range. Dark circles mark the locations determined using 37 stations within 110 km, squares illustrate the event locations by including 63 stations within 125 km range, and triangles indicate the locations when using data from 79 stations located within 140 km of the center of the SCA box in Figure 4.

Santa Barbara Island Sequence (SBI)

The SCSN catalog contains 604 earthquakes from 1981 to 1997 within the SBI box (33.35° to 33.80°N, 119.30° to 118.85°W), which includes the 1981 Santa Barbara Island ($M_L = 5.3$) earthquake. The SCEC database contains 5992 *P* arrivals and 1855 *S* arrivals from 82 stations located within 125 km of these events. As is typical of other regions in southern California, the number of *P* arrivals picked by the SCSN analysts correlates with event magnitude. For many events there are few *S* picks, for the larger events due mostly to trace clipping and for smaller events due to the fact that *S* arrivals are not read routinely for many of the SCSN stations.

We begin by first locating the events with data from the original SCSN picks and the *oce1*, *oce3*, and *oce5* velocity models (see Figure 2). From these initial locations we determine 100 nearest neighbors of each event, as described in Astiz *et al.* (2000). We apply cross-correlation to the *P* and *S* waveforms (see Table 1), from which we determine differential time delays among the events. These times are combined with the original pick times to obtain an adjusted and expanded set of 6490 *P* and 2859 *S* picks (see Shearer, 1997, for details regarding this process). For about 15 events with $M > 3.2$, we first manually picked additional *P* and *S* times to supplement the SCSN picks, which significantly increased the number of stations included in our locations for these events. Since the waveforms from many larger events do not correlate well with those of smaller events, these additional picks could not be obtained through the cross-correlation analysis. The set of adjusted and expanded picks resulting from the original SCSN picks, the manual picking of the larger events, and the waveform cross-correlation was then used to relocate all of the events. Although the increase in the total number of picks is minimal for the Santa Barbara Island sequence, this new set of arrival times now includes data from 63 stations instead of the original 42. Most *P* and *S* station terms for the final locations are within ± 0.5 sec.

It is difficult to discriminate between the different velocity models on the basis of the travel-time residuals returned by the location procedure; each of the three models produces median *P* and *S* travel-time residuals of about 0.06 sec and 0.15 sec, respectively. Some differences are apparent, however, in the standard-error estimates from the different models. Table 3 lists the mean and median errors (*herr*, *zerr*) for the initial and final locations using the three velocity models mentioned above. The median *herr* is about 430 m for each of the models; however, the smallest *zerr* is obtained for the *oce1* model. The results from this model are our preferred locations, since they also include the largest percentage of events (76%) with *herr* ≤ 1 and *zerr* ≤ 2 km.

A comparison between the original SCSN catalog locations and our locations (both before and after waveform cross-correlation) is plotted in Figure 9. In this distributed seismicity example, the improvements in the locations are more subtle than shown previously for the Santa Catalina quarry. Nonetheless, somewhat tighter clustering of the events is seen in the map views (particularly along the southwest edge of the main sequence) and the depths are much

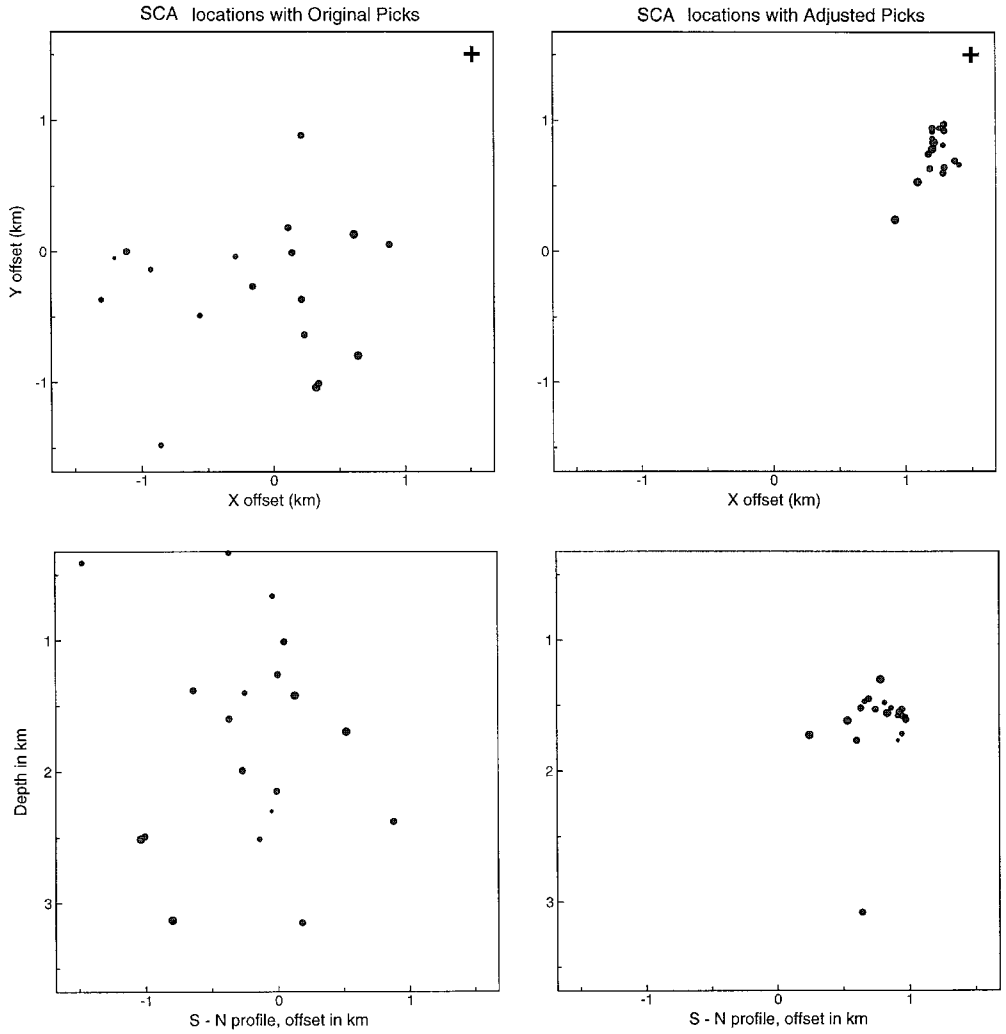

Figure 8. Comparison between the L-1 norm grid-search locations for the Santa Catalina Island events obtained from the original SCSN picks (left panels) and those determined with the adjusted picks resulting from the cross-correlation procedure described in the text (right panels). The cross near the top right corner of the upper map-view panels indicates the Santa Catalina Island quarry location. The bottom panels display S-N cross-sections.

Table 3
Horizontal (*herr*) and Vertical (*zerr*) Errors in km for SBI Events

	SCEC Picks				Adjusted Picks			
	Mean		Median		Mean		Median	
Velocity Model	herr	zerr	herr	zerr	herr	zerr	herr	zerr
*oce1*_125	0.8061	1.7895	0.4690	1.0760	0.7248	1.5123	0.4290	0.7950
*oce3*_125	0.7780	1.8248	0.4550	1.0810	0.7141	1.5916	0.4280	0.8425
*oce5*_125	0.7962	2.0755	0.4610	1.3050	0.7527	1.8393	0.4345	1.1330

better resolved. Our best locations (*herr* $\leq$ 1 and *zerr* $\leq$ 2 km) are plotted in Figure 10, with focal mechanisms for events with $M > 3.8$ taken from Corbett (1984). Note that the western edge of the fault plane is very well defined, both in map view and cross-section, and agrees with the orientation of the focal mechanism solutions and aligns with the eastern escarpment of the Santa Cruz–Santa Catalina Ridge fault. The small cluster of events to the southeast of the main fault (east-southeast of Santa Barbara Island) appear to align along a northwest trend, suggesting an additional parallel

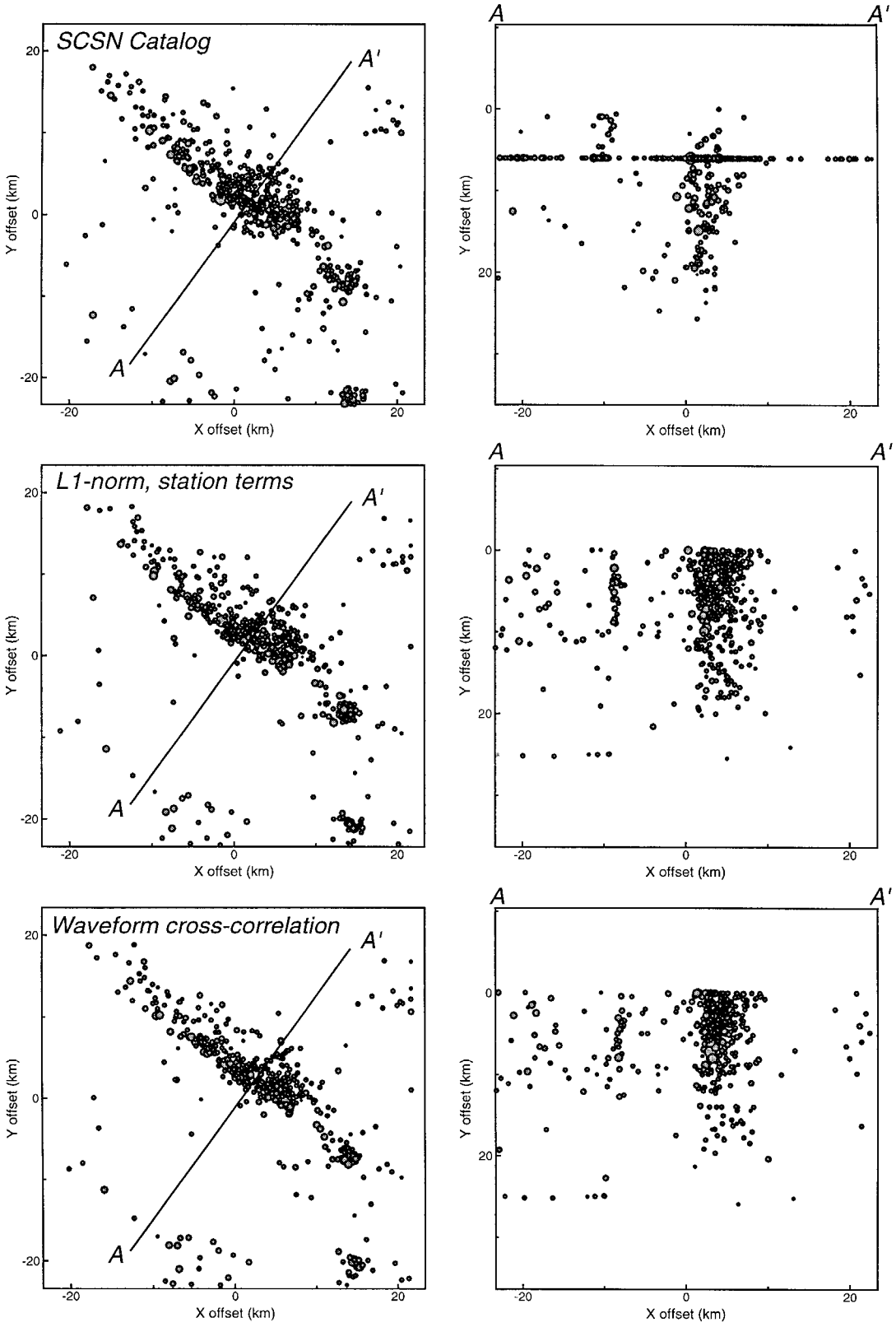

Figure 9. A comparison for events near Santa Barbara Island of the original SCSN catalog locations, with those obtained using the L1-norm and station terms, both before and after waveform cross-correlation. The right panels show cross-sections along the *A*-*A′* profile.

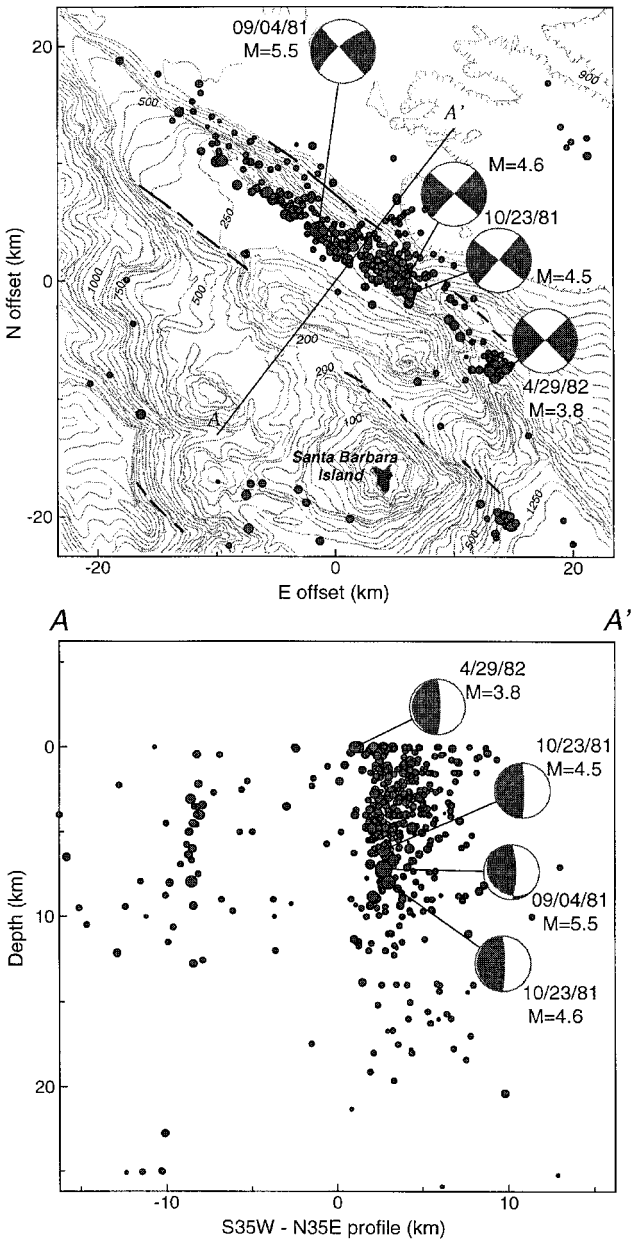

Figure 10. A map view of our final locations near Santa Barbara Island (using the adjusted picks derived from waveform cross-correlation) relative to a reference location of 33.635°N, 119.075°W. Bathymetry and known late Quaternary faults are shown for reference. The lower panel shows the cross-strike vertical cross-section *A*-*A*′. The *oce1* velocity model is used, with data from 63 stations located within 125 km of the events. Only 445 events are shown, those with median standard errors *herr* $\leq$ 1 and *zerr* $\leq$ 2 km (i.e., about 76% of all located events). Bathymetric 50 m contours (National Ocean Survey, 1975), and mapped faults (Kennedy *et al.,* 1987) are plotted in the map view. Focal mechanisms (Corbett, 1984) for events with $M > 3.8$ are lower hemisphere projections in the top panel and their corresponding projections onto the cross-section in the lower panel (i.e., the far hemisphere is plotted).

vertical fault that coincides with unnamed Holocene faults mapped to the east of Santa Barbara Island by Jennings (1994). Estimated standard errors in depth for events in this cluster are 0.5 to 1.5 km; thus the approximately 5-km-vertical extent of this fault appears well resolved.

Figure 11 shows map views of the 1981 Santa Barbara Island earthquake sequence for several time intervals. During the first five months (top panels), the aftershock activity was limited to a region 25-km long in the vicinity of the mainshock. The activity decreased dramatically in this region in the following two months, moving to the small northwest trending fault to the southwest of the initial activity. During April 1982 the aftershock activity shifted back to the Santa Cruz–Santa Barbara Ridge fault zone extending the seismicity more to the southeast. Seismicity in this region has been low (less than 4 events per year) since May 1983, concentrating along the main fault zone.

Corbett (1984) located 458 aftershocks occurring within 2 years of this event, using an $M_L = 2.8$ event located near the center of the sequence on September 21, 1981, as the master event. His locations for events in the 1981 Santa Barbara Island earthquake sequence are very similar to those obtained in our study, but are overall about 4 to 5 km deeper than our final locations. Accurately constraining absolute event depth for these offshore events is very difficult due to the uneven station coverage, possible lateral velocity variations in the source region, and uncertainties in choice of the 1D reference model. Corbett (1984) estimated that his absolute depths may be off by as much as ± 5 km; our experiments with different velocity models suggest that our absolute depths could be off by up to ± 3.5 km.

Figure 12 compares station terms of *P* and *S* waves resulting from the master event locations of Corbett (1984) for the 1981 Santa Barbara Island sequence and those from our final locations. Note the similarity in the patterns for both *P* and *S* waves between these studies, with positive *P* and *S* station terms along the Transverse Ranges and mostly negative station terms for the Los Angeles Basin. We used roughly three times more stations in our locations than the Corbett study, but obtained generally smaller values for the final station terms.

The 1986 Oceanside Sequence (OCS)

The SCSN catalog contains 3215 events that occurred from 1981 to 1997 within the OCS box (32.8° to 33.2°N, 118.0° to 117.6°W) shown in Figure 4. Most of these events are aftershocks of the July 7, 1986, Oceanside ($M_L = 5.3$) earthquake. As before, we first applied the L1-norm grid-search algorithm to these events using the original SCSN picks: 28,064 *P* and 8721 *S* arrivals from 66 stations located within 125 km. We were careful to include data from all island stations in order to obtain the best possible azimuthal coverage. We required a minimum of five picks to locate an event, thus only 88% of the events are included. The events are located with three of the velocity models shown in Figure 2, yielding similar mean and median *herr* and *zerr* errors for

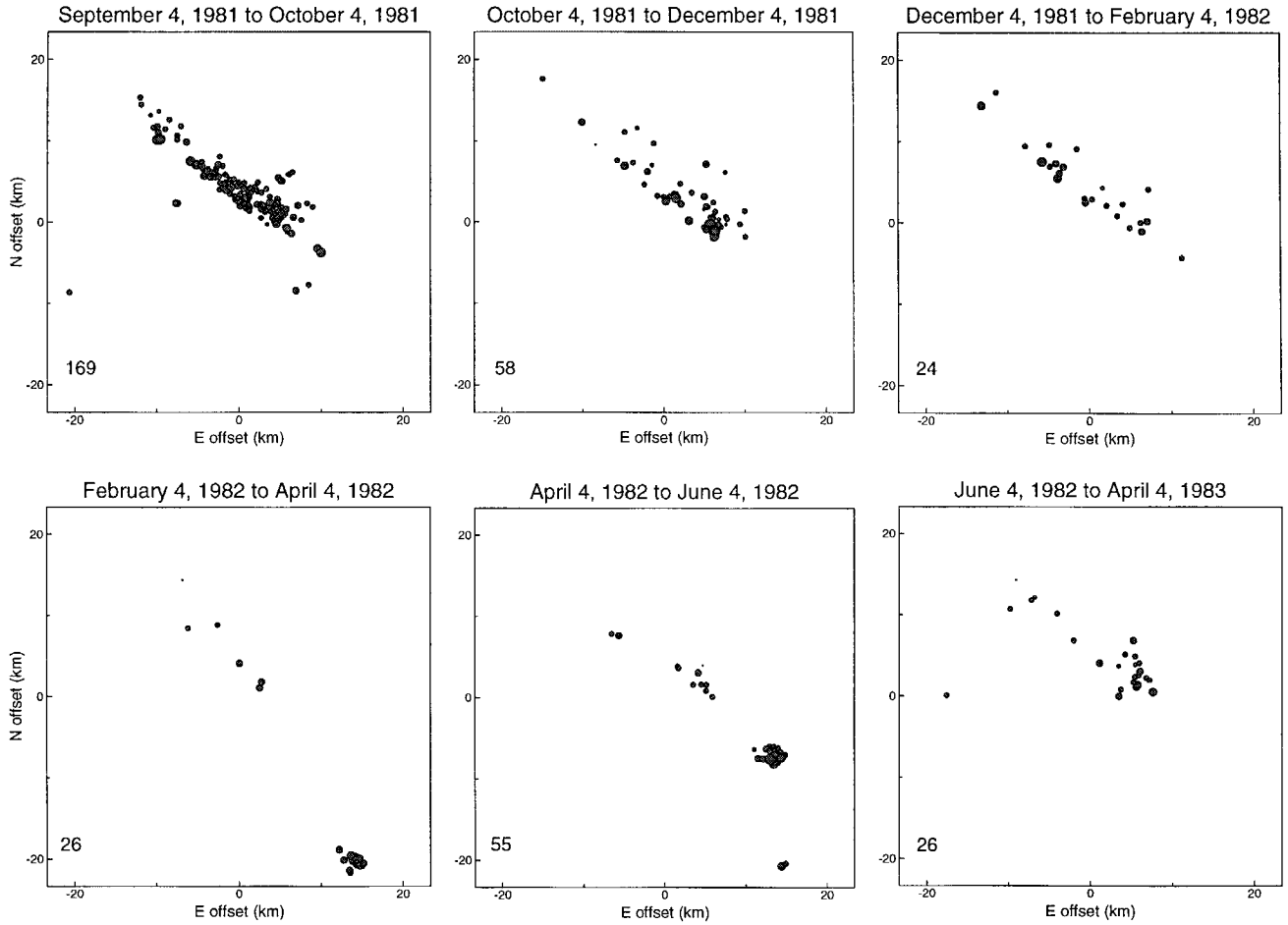

Figure 11. Time slices of the best-located events that occurred 18 months after the 1981 Santa Barbara Island earthquake. Time intervals are indicated above each map view. The number of events in each panel is given in the lower left corner.

the initial runs (Table 4). Since many of the larger magnitude events do not cross-correlate well with smaller events, in part due to instrumental clipping or to the fact that waveforms of larger events may be more complex, we hand-picked *P* and *S* arrivals for missing stations for about 30 of the largest events. For comparison with the locations obtained from the SCSN picks alone, we relocated 156 events with $M > 3.0$ using the increased pick set. The median errors decreased from about 520 m to 320 m for *herr* and from 700 m to 400 m for *zerr* (see Table 4).

From the initial locations of all the events we determine each of its 100 nearest neighbors. Next we apply cross-correlation to 2-and 3-sec-long windows around the *P*- and *S*-arrival times (see Table 1) to determine time delays among the events, which we then use to adjust the existing picks to obtain a total of 30,184 *P* and 15,060 *S* adjusted arrivals. The histograms in Figure 13 show the change in the number of *P* and *S* picks from the original SCSN analyst picks (light bars) to those obtained after cross-correlation (dark bars). Note that about 45% of the events had fewer than three *S* picks in the original data; however, after our cross-correlation and time-adjustment procedure only 10% of the events had fewer than three *S* picks. The events are then relocated using the adjusted set of picks, using the station term values obtained from relocating the largest events as initial values in our relocations.

A map view and cross-section from the results of three of our locations are shown in Figure 14. At the top are the initial L1-norm locations using the original SCSN picks. The middle panels display the result of applying the L1-norm algorithm only to events with $M > 3.0$. The bottom panel shows locations using adjusted picks and the station terms estimated from the location of $M > 3.0$ events as initial values. The *oce1* velocity model is used in all three locations, with data from stations within 125 km range. Notice that the locations computed from the adjusted picks (Fig. 14, bottom) appear more tightly clustered than the locations derived from the original picks (Fig. 14, top). The cross-section in the middle panel images most clearly a northeast-dipping fault plane that may shallow at depth. A north-dipping fault plane is consistent with Pacheco and Nábêlek's (1988) interpretation of the Oceanside earthquake, in contrast to that of

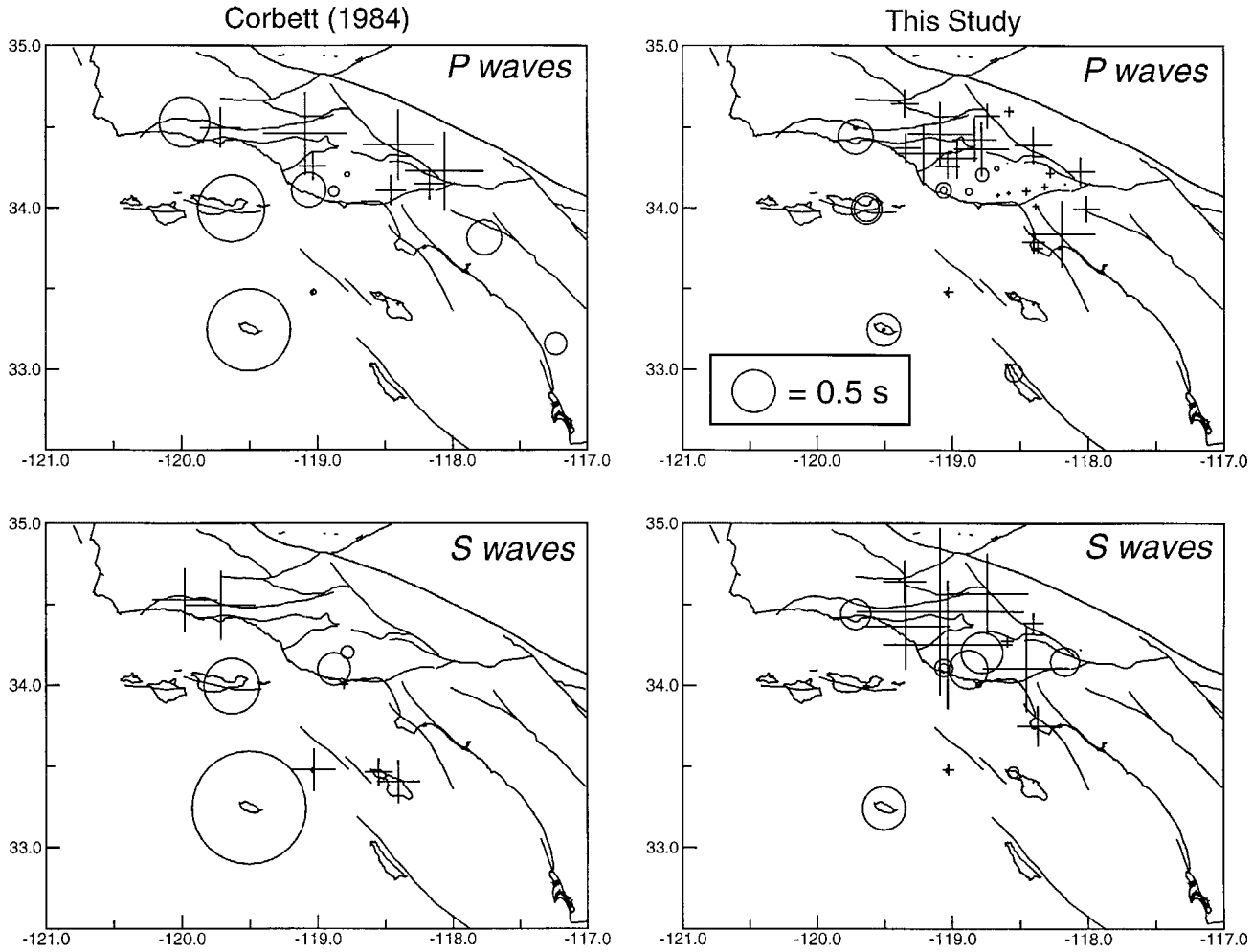

Figure 12. Comparison of *P*-wave (top) and *S*-wave (bottom) station terms resulting from the master event locations of Corbett (1984) for the 1981 Santa Barbara Island sequence (left panels) and those from our final locations after performing waveform cross-correlation (right panels). Note the similarities in the variation of the patterns and the larger number of stations used in our study, about a factor of 3 more. Crosses are positive residuals and circles are negative residuals; symbol size is proportional to the amplitude of the station term.

Table 4
Median Horizontal (*herr*) and Vertical (*zerr*) Errors in km for OCS Events

	Scec Picks				Adjusted Picks			
	All events		M < 3.0 events		Starter 0 = 0.0		Modified starter 0	
Model	herr	zerr	herr	zerr	herr	zerr	herr	zerr
*oce1*_125	0.5220	0.7320	0.3225	0.4220	0.4280	0.5700	0.4310	0.5610
*oce3*_125	0.5210	0.6810	0.3155	0.3815	0.4220	0.5840	—	—
*oce4*_125	0.5670	0.6810	0.3255	0.4660	0.4570	0.5700	—	—

Hauksson and Jones (1988) who suggested that a south dipping plane was implied by their locations (see their Figure 8). However, the dip of the plane imaged is about 30°, which is nearly 20° shallower than that obtained both by the first-motion focal mechanism of the event (Hauksson and Jones, 1988) and teleseismic-waveform modeling (Pacheco and Nábêlek, 1988).

Figure 15 shows a map view and cross-section of our final locations (using the *oce3* model, initial station terms from the location of the largest events, and adjusted picks

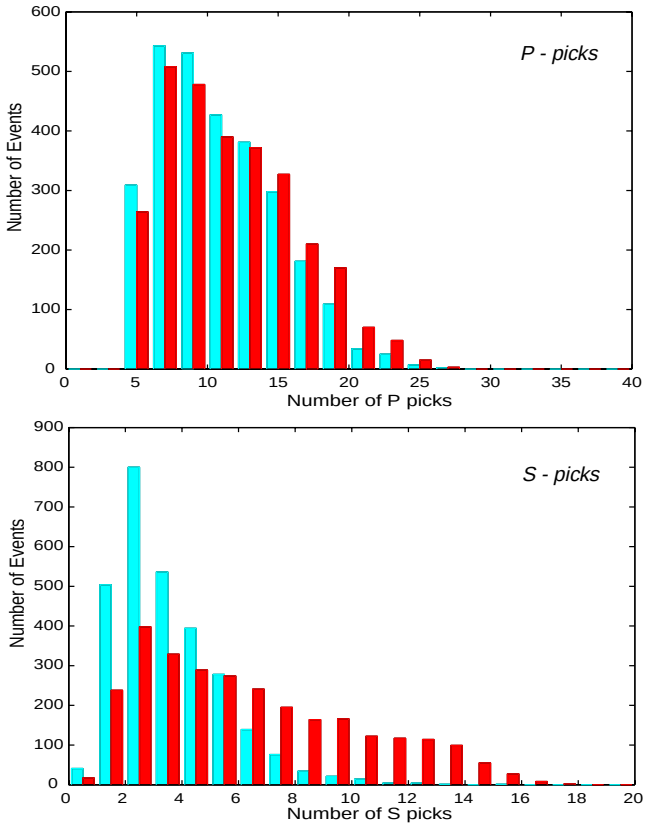

Figure 13. Number of *P* (top) and *S* picks (bottom) from stations located within 125 km of the Oceanside region. Light bars are for the original SCSN catalog and dark bars are the adjusted arrival times obtained after waveform cross-correlation with the 100 natural neighbors to each event. The number of *P* picks increases from the original 28,064 to 30,184; the *S* picks increase almost two fold from the original 8,721 to 15,060 after cross-correlation.

from 66 stations located within 125 km of the events). The lower panel shows the vertical cross section along *A*-*A*′. We plot 2378 events, with median standard errors *herr* $\leq$ 1 and *zerr* $\leq$ 2 km (about 75% of our locations). The events lie beneath a bathymetric high, with strike similar to our event locations, at the northern edge of the San Diego Trough–Bahia Soledad fault zone. Mann and Gordon (1996) suggest that this bathymetric high is the product of a gentle restraining bend as the strike of the fault changes in the inner Continental Borderland. Focal mechanisms for events with $M > 3.8$ (Hauksson and Jones, 1988) are plotted as lower hemisphere projections in the top panel and their corresponding far-side projections onto the cross section in the lower panel. Larger aftershocks indicate thrusting with a strike-slip motion, consistent with the regional tectonics of the San Andreas fault system in southern California (Weldon and Humphreys, 1986; Feigl *et al.*, 1993). The thrust-faulting mechanism of this event may also indicate weak strike-slip faults offshore, similarly to the 1983 Coalinga (M_L = 6.4) and the 1984 Avenal (M_L = 5.7) thrust-faulting earthquakes that occurred near the San Andreas fault in central California (Mount and Suppe, 1987; Zoback *et al.*, 1987). Seismicity before the 1986 Oceanside earthquake in this region was diffuse (~20 events per year). The aftershock distribution over time did not change significantly, showing a similar distribution to that of the whole sequence as shown in Figure 15.

Although our locations are much more clustered than those obtained in previous Oceanside aftershock studies, and clearly define a northeasterly dipping fault plane, the best located aftershocks (see Figure 15) outline a broad zone about 4-km thick. Thus we cannot distinguish if all the events are associated with a single fault, or more likely, with a series of faults in a rather complex structure. If all events occurred within a single fault zone, the mislocations could be due to extreme variations in the velocity structure in this region that we fail to account for in our location procedure. However, it is also possible that the broad zone reflects a series of faults associated with the change of strike of the San Diego Trough–Bahia Soledad fault zone to the Santa Catalina Fault Zone (see Figure 4).

Seismicity near Coronado Bank (CBK)

There are 104 events in a box (32.37° to 32.72°N, 117.50° to 117.20°W) around the Coronado Bank region (CBK in Figure 4) listed in the SCSN catalog between 1981 and 1997. The seismicity rate in this region has been low (four to six events per year) with the exception of a sequence of 22 small earthquakes that followed the 1986 Oceanside (M_L = 5.3) earthquake. These earthquakes occurred mainly in August 1986, with four of them having M_L between 3.0 and 3.7. The SCSN analysts picked 816 *P* and 309 *S* arrivals for these events. Since the CBK region is very close to the coast, we decided to relocate the events using two different station ranges: 110 and 130 km with all five velocity models shown in Figure 2. We included island stations regardless of their range whenever possible to ensure that we had stations surrounding this region. Following the initial locations, we window the waveform data around the expected *P*- (−0.75 to 1.75 sec) and *S*- (−0.75, 2.75 sec) arrival times to estimate cross-correlations between each event and all other events in the region, and then, as before, use these differential times to solve for a new set of picks. Although we only increased the original *P*-(834) and *S*- (364) arrival data slightly, we refined the existing picks and obtained more data for the critical island stations.

Figure 16 shows a comparison between the original SCSN *P* picks for a "tree" of 10 Coronado Bank events recorded by station CIS and adjusted picks provided by an inversion that included differential times obtained with waveform cross-correlation. We use these adjusted picks for the final relocations. Table 5 lists the median horizontal (*herr*) and vertical (*zerr*) errors resulting from relocating these events for the different velocity-station distance combinations. Note that the median *herr* decreases for locations that include stations from 110 to 130 km but the *zerr* become

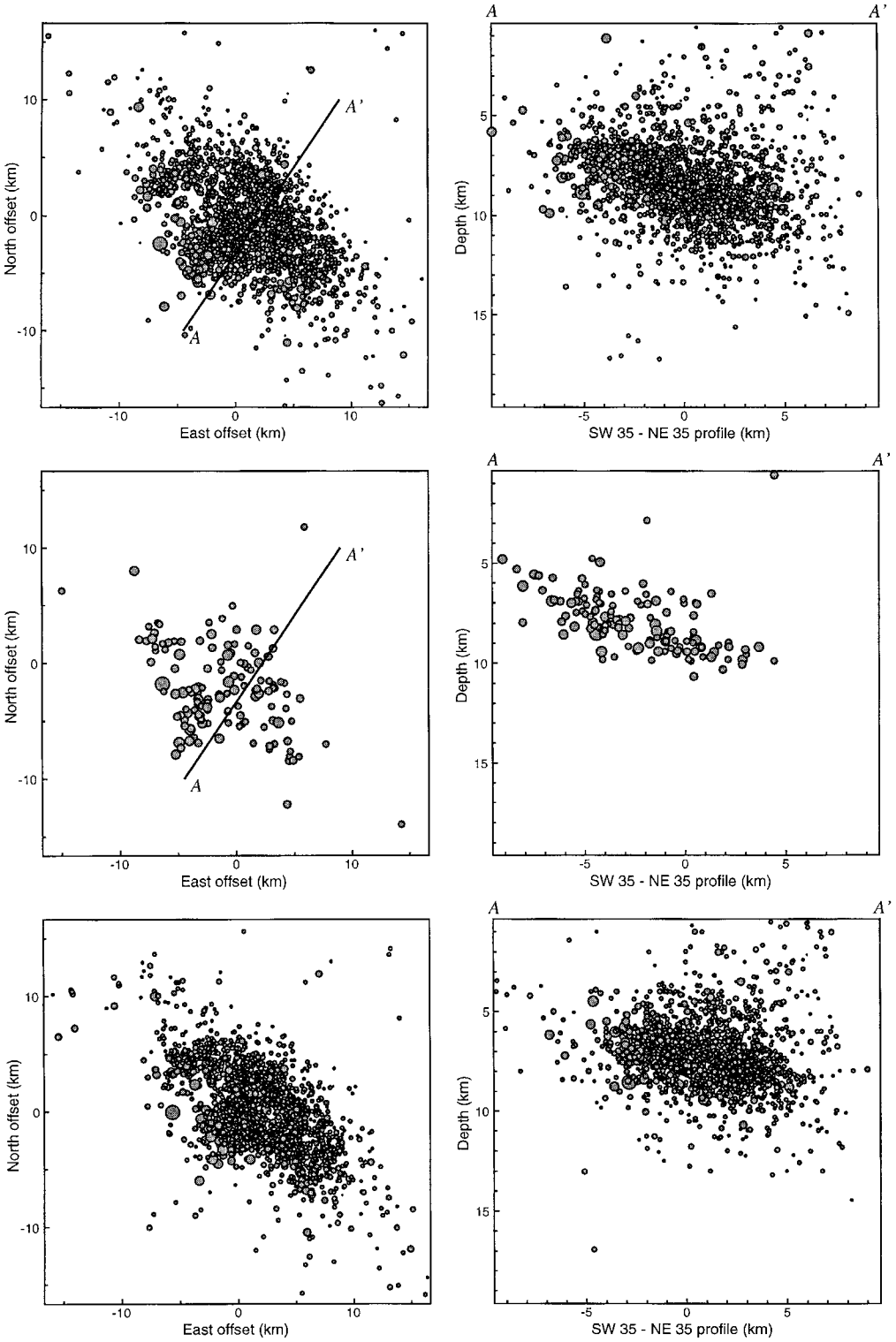

Figure 14. The top panels show a map view and cross-section (*A*-*A*′) of our initial L1-norm locations using the original SCSN picks for the Oceanside sequence. The middle panels display the result of applying the L1-norm grid-search algorithm only to events with $M > 3.0$. The bottom panel shows locations using the new set of adjusted picks. The reference location in all panels is 33.00°N and 117.78°W; we show events with *herr* < 0.75 and *zerr* < 1.5 km. For these locations we use data from stations within 125 km and the *oce1* velocity model.

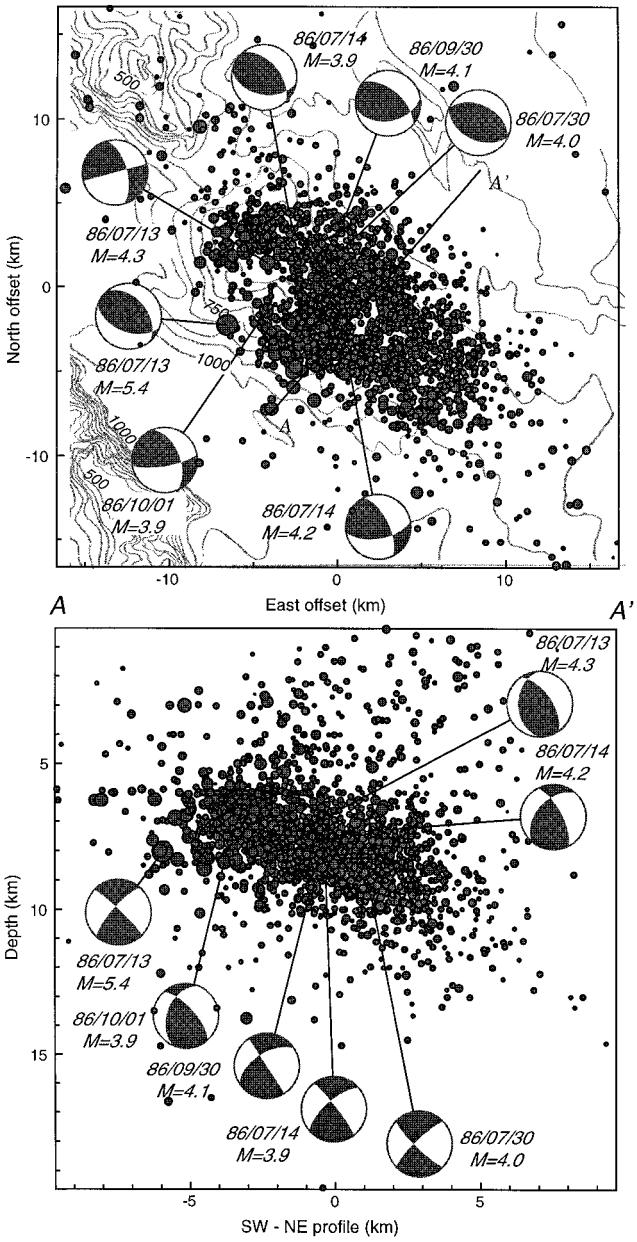

Figure 15. The top panel is a map view of our final locations for the Oceanside sequence with the adjusted picks from 66 stations located within 125 km of the events. The reference location is 33.00°N and 117.78°W. We use the *oce3* velocity model and the station terms from locations of events with $M > 3.0$ as initial values. The lower panel shows the cross-strike, vertical cross-section *A*-*A*′. We show 2378 events, with median standard errors $herr \leq 1$ and $zerr \leq 2$ km (about 75% of the events). Light gray lines are 50-m bathymetric contours (National Ocean Survey, 1975). Focal mechanisms for events with $M > 3.8$ (Hauksson and Jones, 1988) are lower hemisphere projections in the top panel and their corresponding projections onto the cross section in the lower panel (i.e., the far hemisphere is plotted).

larger. The station terms do not show a dependence on range for any of the relocations; however, for island stations they increase from about -0.1 sec to as much as -1.0 sec from those relocations taking into account inland stations located within 110 or 130 km range. Since station terms are only estimated for stations with more than five picks, we include picks from 10 stations at 100 km range and 18 stations for 130 km range relocations. The initial locations with stations to 110 km only include readings from station SCI (San Clemente Island), but for all other locations we also include picks from station CIS (Catalina Island). Although we obtain similar map view projections for locations with different velocity models, the overall event depth distribution varies. For the same velocity model, locations with stations to 110 km tend to be deeper and further from the coastline than those including inland stations located within 130 km.

Our final locations use the *oce4* velocity model for events with a minimum of 4 *P* and 2 *S* picks and include inland stations within 110 km distance and data from the SCI island station. The overall errors are $herr = 590$ m, $zerr = 522$ m, smaller than those listed in Table 5. Station terms for both *P* and *S* waves are within ± 0.3 sec. The map view of our final locations, which use the adjusted picks, is shown in the top panel in Figure 17. We plot 65 events, those with median horizontal and vertical standard errors less than 1.5 km. The map view shows bathymetry (National Ocean Survey, 1975) and fault traces (Kennedy *et al.*, 1987) and our event locations for this region, which are located nearly 10 km further east than the original SCSN catalog locations. Some of the events have a northwesterly trend that parallels the Coronado Escarpment and Loma Canyon to the west, whereas other events show a northeasterly direction parallel to Coronado Canyon. The bottom panel shows a SW–NE profile that clearly indicates that events further from the coastline are shallower than those closer to it. The deepest events have depths around 15 km; similar depths were determined by Magistrale (1993)from location of event clusters occurring in the last six months of 1986 in the San Diego region. He used data from the SCSN together with data from a temporary local array deployed in the San Diego area at that time. Since we only use data from 13 stations to locate the events in the CBK region, which are mostly situated to the northeast of the events, it is possible that there is a mislocation vector associated with the absolute location of these events. Their relative locations, however, should be robust.

San Clemente Island Clusters (SCLN, SCL, SCLS)

The SCSN catalog lists 356 earthquakes that occurred near the San Clemente fault trace from 1981 to 1997, but these events do not form clear spatial or temporal clusters of activity. We divided these events into the three regions near San Clemente Island (SCLN, SCL, SCLS) shown in Figure 4. Our initial locations used the existing SCSN picks and the *oce4* velocity model (which has thinner crust than our other models). To increase the number of pick data available for locating these events, we included all stations within 140

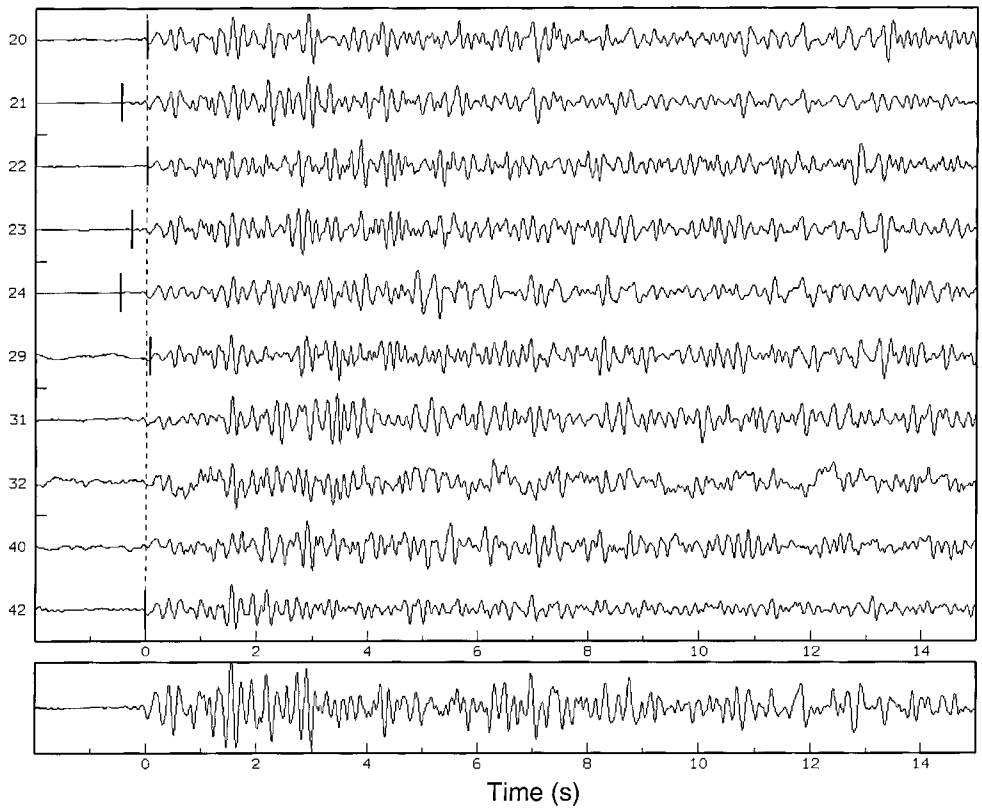

Figure 16. A comparison between the original SCSN *P* picks for a "tree" of 10 Coronado Bank events recorded by station CIS and adjusted picks provided by an inversion that included differential times obtained with waveform cross-correlation. SCSN picks were available for seven of the stations and are indicated by tic marks. The waveforms are aligned on their adjusted picks, shown by the dashed line. The bottom trace is a stack of all the traces above.

Table 5
Median Horizontal (*herr*) and Vertical (*zerr*) Errors in km for CBK Events

	SCSN Picks		Adjusted Picks	
Velocity Model	herr	zerr	herr	zerr
*oce1*_110	0.7595	0.5380	0.6870	0.5790
*oce1*_130	0.6585	0.8260	0.6730	0.5565
*oce2*_110	0.7820	0.4750	0.6230	0.7420
*oce2*_130	0.6160	0.7870	0.6460	0.7100
*oce3*_110	0.7595	0.5140	0.6730	0.5565
*oce3*_130	0.6590	0.6320	0.8845	0.7750
*oce4*_110	0.7345	0.5490	0.6280	0.5580
*oce4*_130	0.7135	0.7975	0.6390	0.6780
*oce5*_110	0.7290	0.5960	0.6730	0.5670
*oce5*_130	0.7130	0.8810	0.6440	0.7150

km range. Next, we determined the 100 nearest neighbors of each event, performed cross-correlation of the *P* and *S* waves with the window parameters listed in Table 1, and computed a new set of adjusted pick times. Since most of the events are not clustered, we increased our initial pick data set only marginally; however, after waveform cross-correlation the consistency of the existing *P* and *S* picks improved, decreasing the horizontal and vertical errors of our final locations (Table 6). Only events with *herr* $<$ 1.5 and *zerr* $<$ 3.0 km are shown in Figure 18, i.e., 63% (SCLN), 61% (SCL), and 34% (SCLS) of the events listed by the SCSN catalog are displayed.

The SCSN catalog lists 56 events in the SCLN region to the north of San Clemente Island, but only 38 had more than 5 picks. Note that most of the events in the map shown in Figure 18 locate near the traces of known fault scarps such as the San Clemente fault, east of the island, as indicated by the bathymetry. In the vertical cross-section, the events appear to delineate two vertical faults. For this region we use data from 38 stations; the closest is San Clemente Island (SCI) located approximately 21 km away from the bulk of the events. After the cross-correlation procedure we increased the original *P* and *S* data by 10 and 8 more picks, respectively. The relative horizontal and vertical median errors of our locations are of the order of 1 and 2 km (see Table 6). The 24 events shown in the top panels have *herr* $<$ 1.5 and *zerr* $<$ 3.0 km.

The region encompassing the southern portion of San

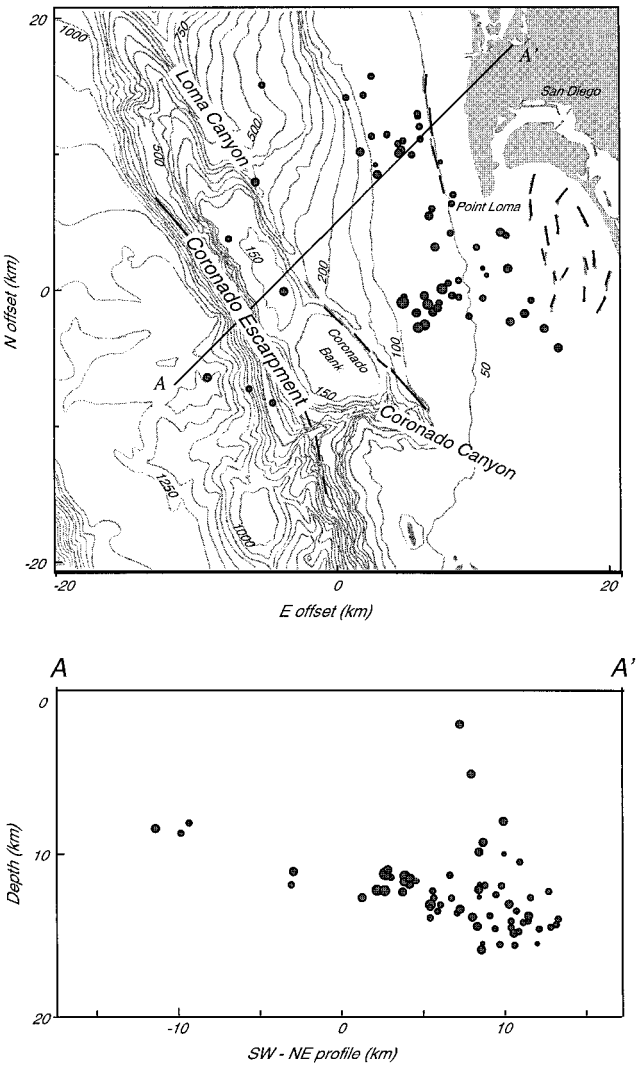

Figure 17. Map view of the final locations of Coronado Bank events using the adjusted picks displayed in the top panel. The reference location for the events is 32.60°N and 117.36°W. Bathymetry in 50-m contours (National Ocean Survey, 1975), and some mapped faults (Kennedy *et al.*, 1987) are shown. We plot only 61 events, those with *herr* and *zerr* $\leq$ 1.5 km. The bottom panels show a vertical cross section along the *A*-*A′* line in the top panel.

Table 6
Horizontal (*herr*) and Vertical (*zerr*) Errors in km for San Clemente Events

	SCEC Picks				Adjusted Picks			
	Mean		Median		Mean		Median	
Region	herr	zerr	herr	zerr	herr	zerr	herr	zerr
SCLN	2.0826	2.9137	1.7590	2.6260	1.8469	2.3198	1.0505	1.9200
SCL	1.9199	1.7420	1.1275	1.3380	1.9161	1.9842	1.1120	1.3125
SCLS	2.3568	2.6961	1.8635	2.2200	2.2518	2.6264	1.8325	2.0995

Clemente Island (SCL), included 81 events in the SCSN catalog but only 60 events had more than 5 picks. Our best locations of these events are shown in the middle panels of Figure 18. The map view shows bathymetry (National Ocean Survey, 1975) and fault traces (Kennedy *et al.*, 1987). Note that most of the events in this region follow the trend of the San Clemente fault. In cross-section the events locate throughout the crust, suggesting the presence of a vertical fault. We use pick data from 21 stations for this region. Although the location errors are only slightly higher than in the previous region (see Table 6), absolute depth resolution is questionable since the closest station is SCI, and the next closest station is about 60 km away from the events. We used 378 and 106 *P* and *S* picks, increasing to 384 and 126 adjusted picks after the cross-correlation procedure. After the cross-correlation procedure with a 3-s *P*-wave window and a 4-s *S*-wave window we obtained about one more *P* pick for every ten events, but nearly one more *S* pick for every three events.

Figure 18 also shows final locations for events within the region located southeast of San Clemente Island, between the San Clemente basin and the Fortymile Bank regions. The SCSN catalog lists 219 events, but only 34% of these events are included in our best locations shown in Figure 18. The map view suggests that events in the SCLS region may be associated with different strands of the San Clemente fault (Kennedy *et al.*, 1987). However, in cross-section they do not clearly delineate either a single fault or a series of simple faults. Median horizontal and vertical errors for events in this region are near 2 km, probably due to the fact that the closest recording station is about 60 km away and the second one about 90 km away from these events.

Discussion

Locating earthquakes in the Continental Borderland offshore Southern California is problematic, due to the asymmetrical distribution of stations that record these events and the uncertainties in the local velocity structure. The lack of nearby recording stations for many of the regions for which we located earthquakes (see Figure 4) implies that the absolute (mean) location of each cluster of events is difficult to constrain precisely, particularly in depth. Nonetheless, by using the L1-norm location method of Shearer (1997), waveform cross-correlation to improve and enlarge the set of arrival time picks, and customized station terms for each region, we are able to obtain good relative locations among nearby events. Our locations compare favorably to previous results obtained using a master event method for aftershocks of the Santa Barbara Island (M_L = 5.3) earthquakes along the Santa Cruz–Santa Catalina fault (Corbett, 1984). We locate probable quarry blasts on Santa Catalina Island into a tight cluster within a few kilometers of the actual site of the Santa Catalina quarry. Estimated mean relative location errors for the highly repeatable events within this cluster are

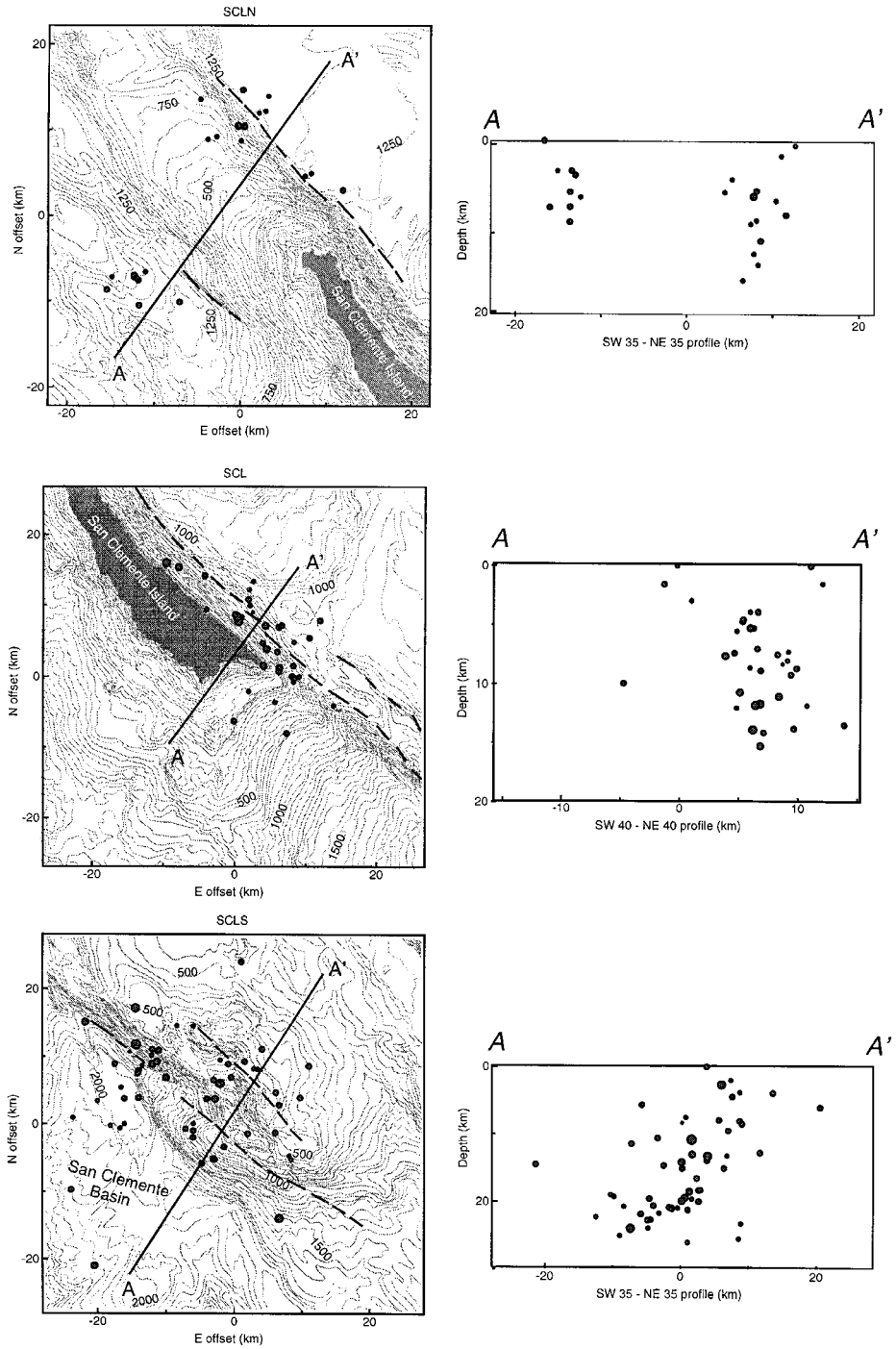

Figure 18. The left panels show map views of our final locations using the adjusted picks from stations located within 140 km of the events and the *oce4* velocity model for the three regions located near San Clemente Island. The panels to the right show vertical cross-sections (*A*-*A*′) normal to the strike of known fault lineations in this region. The top panels display final locations for the SCLN region, relative to a reference location of 33.06°N and 118.67°W, the middle panels show locations for the SCL region referenced to 32.80°N and 118.40°W, and the lower panels show locations for events within the SCLS region with reference location of 32.60°N and 118.00°W. All panels show events with *herr* $<$ 1.5 and *zerr* $<$ 3.0 km. Only 63% (SCLN), 61% (SCL), and 34% (SCLS) of the events found in the SCSN catalog located within these errors. Faults (from Kennedy *et al.*, 1987) and 50 m bathymetric contours are also shown.

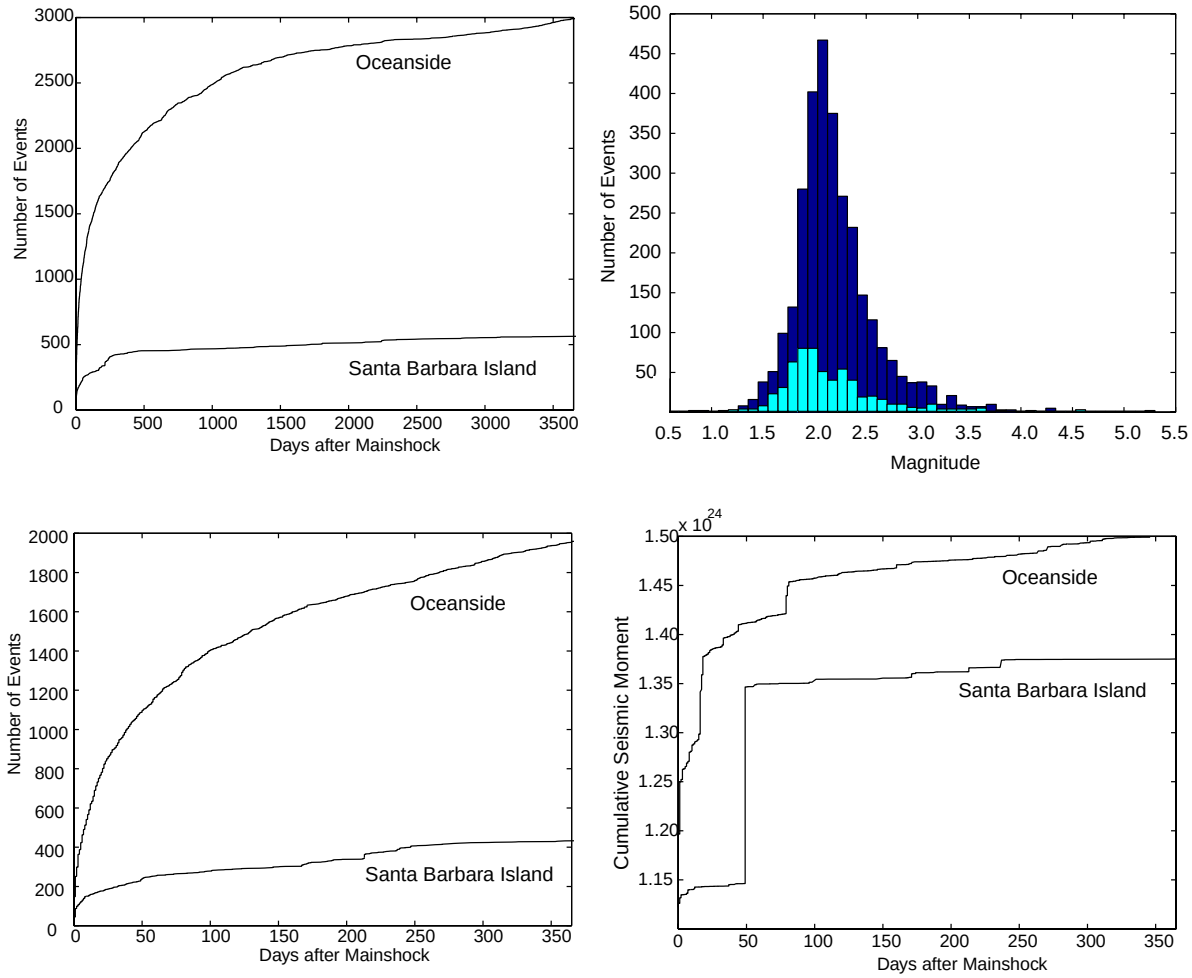

Figure 19. The left side panels show the time distribution of number of events for the Oceanside and Santa Barbara Island regions. Both the ten-year period (upper) and the one-year period (lower) show that the Oceanside sequence has 5 times more events than the Santa Barbara Island event. The histograms on the upper right show the magnitude distribution of the Oceanside events with black bars and that of the Santa Barbara Island event with gray bars. The lower right panel shows the cumulative seismic moment from the one-year aftershocks after each mainshock.

60 to 90 m, comparable to results obtained for inland clusters in southern California using the same technique. In contrast, estimated relative location errors for other offshore regions are at least an order of magnitude larger than those for the Santa Catalina events (see Tables 3 to 6).

The relocated events in the regions in this study, with the exception of the SCA region, tend to cluster around mapped fault scarps or within transpressional fault regions slightly oblique to the direction of the plate motion that may contain gently restraining bends. Events occurring in the SBI, SCLN, SCL, and SCLS regions are clearly associated with northwest trending strike-slip faults consistent with a broad zone of right-slip deformation associated with the San Andreas fault system in southern California (e.g., Hutton *et al.*, 1991). Locations for events near the Coronado Bank region (CBK) do not seem to align near obvious bathymetric features, such as the Coronado Escarpment, but occur at 10 to 15 km depth along an apparent northeast dipping fault close to the San Diego coast (see Figure 17). The 1986 Oceanside earthquake and its aftershocks are located at the northern end of the San Diego Trough (see Figure 1) and exhibit a more complex pattern of faulting (see Figure 15). Hauksson and Jones (1988) proposed that these events may have occurred in a small fault that provides a left step of the San Diego Trough fault as it curves around the Santa Cruz–Catalina escarpment (see Figure 4). Although they chose a south-dipping plane as the fault plane of the Oceanside event, their best locations do not seem to delineate unambiguously either a north- or a south-dipping plane (see their Figures 7b and 8b). In contrast, our final locations clearly show a northeast dipping fault plane, in agreement with the interpretation of Pacheco and Nábêlek (1988).

It is interesting that our locations for both the Oceanside sequence and the offshore San Diego events near Coronado

Bank suggest faults dipping gently to the northeast. It is possible that these faults are shallow-angle thrust or detachment faults, such as the Oceanside detachment fault seen in offshore reflection seismic data and proposed by Crouch and Suppe (1993) and Bohannon and Geist (1998) to mark the boundary between the Peninsular Range belt to the east and the Catalina Schist belt to the west. To evaluate this possibility, a more detailed comparison between offshore seismic reflection profiles and the natural seismicity should be performed. If the Oceanside and/or Coronado events indeed occurred on portions of a much larger system of offshore thrust faults, this would have important implications because it would establish that these faults are seismically active and a potential source of large future offshore events.

Although the 1981 Santa Barbara Island and the 1986 Oceanside earthquakes had the same magnitude ($M_L = 5.3$), the number of aftershocks for Oceanside is about a factor of five larger than for the Santa Barbara Island event. In addition, the Oceanside region shows a high level of aftershock activity even after 1500 days (about four years) of the mainshock, whereas the number of events occurring in the Santa Barbara Island region decreased considerably within 500 days of the mainshock. This difference is almost an order of magnitude larger for the Oceanside sequence during the first year after the mainshock (Fig. 19). On the other hand, the magnitude distribution of the Oceanside and that of the Santa Barbara Island event, suggest that the magnitude detection level is similar for both sequences or may be even smaller for the 1981 event. However, when we plot the cumulative seismic moment release for both sequences, the difference between them is not so striking, as shown in Figure 19. We estimated the seismic moment of each event using the moment-magnitude relation of Kanamori and Anderson (1975). Note that for the 1981 earthquake most of the seismic moment was released by the two large aftershocks with $M_L \sim 4.6$, that occurred nearly two months after the main event. The Oceanside event had its largest aftershock ($M_L = 4.3$) within hours of the mainshock, with the next largest event occurring about two weeks later.

Our earthquake locations in the inner Continental Borderland region generally indicate that seismicity is associated with mapped Quaternary faults (Jennings, 1994). This correlation is consistent with evidence that tectonic stress is accumulating in this complicated region, as shown by recent GPS measurements between San Clemente Island and San Diego (Feigl *et al.*, 1993). The observed seismicity indicates that faults within this region are active and may be capable of generating earthquakes of $M_L \sim 6.0$ as suggested by earlier workers (e.g., Agnew, 1979; Legg, 1989; Hutton *et al.*, 1991) and required by recent kinematic models for southern California (Weldon and Humphreys, 1986; Atwater and Stock 1998).

Acknowledgments

We thank the personnel of the USGS/Caltech Southern California Seismic Network who pick and archive the seismograms and to the Southern California Earthquake Center for their distribution, and especially Katherine Hafner who facilitated access to the database. We thank P. Wessell and H. F. Smith (1991) for the generous distribution of the GMT program that was used to generate maps in this study. Large-scale bathymetric data were provided by Stu Smith of the Scripps Data Center. We thank Mark Legg for discussions and for comments on an earlier version of this manuscript. Detailed and constructive reviews by Rob Crosson, Doug Dodge, and Jose Pujol were also very helpful. This research was supported by the Southern California Earthquake Center. SCEC is funded by NSF Cooperative Agreement EAR-8920136 and USGS Cooperative Agreements 14-08-001-A0899 and 1434-HQ-97AG01718. The SCEC contribution number for this paper is 490. Funding for this research was also provided by NEHRP/USGS grants 1434-94-G-2454 and 1434-HQ-97-GR-03162.

References

Agnew, D. C. (1979). Tsunami history of San Diego, *San Diego Assn. Geol. Rept.*, 117–122.

Agnew, D. C. (1990). The use of time-of-day seismicity maps for the earthquake/explosion discrimination by local networks, with an application to the seismicity of San Diego County, *Bull. Seism. Soc. Am.* **80,** 747–750.

Allen, C. R., L. T. Silver, and F. G. Stehli (1960). The Agua Blanca fault—A major transverse structure of northern Baja California, Mexico, *Geol. Soc., Am. Bull.* **71,** 457–482.

Aster, R. C., and J. Scott (1993). Comprehensive characterization of waveform similarity in microearthquake data sets, *Bull. Seism. Soc. Am.* **83,** 1307–1314.

Astiz, L., P. M. Shearer, and D. C. Agnew (2000). Precise relocations and stress-change calculations for the Upland earthquake sequence in southern California, *J. Geophys. Res.*, in press.

Atwater, T. M. (1970). Implications of plate tectonics for the Cenozoic tectonic evolution of western North America, *Geol. Soc. Am. Bull.* **82,** 3518–3536.

Atwater, T. (1989). Plate tectonic history of the northeast Pacific and western North America, in *The Eastern Pacific Ocean and Hawaii, Geology of North America,* v. N, E. L. Winterer, D. M. Hussong, and R. W. Decker, (Editors), Boulder, Colorado, Geological Society America, 21–79.

Atwater, T., and J. Stock (1998). Pacific-North America plate tectonics of the Neogene Southwestern United States: an update, *International Geology Review* **40,** 375–402.

Beyer, L. A. (1980). Interpretation of the gravity map of California and its continental margin: offshore Southern California, in Ed. H. W. Oliver (Editor), *Calif. Div. Mines Geol. Bull. 205,* 8–15.

Billings, S. D., M. S. Sambridge, and B. L. N. Kennett (1994). Errors in hypocenter location: picking, model and magnitude dependence, *Bull. Seis. Soc. Am.* **84,** 1978–1990.

Bird, P. and R. W. Rosenstock (1984). Kinematics of present crust and mantle flow in southern Calif., *Geol. Soc. Am. Bull.* **95,** 946–957.

Bohannon, R. G., and E. Geist (1998). Upper crustal structure and Neogene tectonic development of the California Continental Borderland, *Geol. Soc. Am. Bull.* **110,** 779–800.

Brune, J. N., R. S. Simons, C. Rebollar, and A. Reyes (1979). Seismicity and faulting in northern Baja California, in P. L. Abbot and W. J. Elliott (Editors), *Earthquakes and other Perils—San Diego Region: Geological Society of America Annual Meeting Guidebook,* 83–100.

Clarke, S. H., H. G. Greene, and M. P. Kennedy (1985). Identifying potentially active faults and unstable slopes offshore, *U.S. Geol. Surv. Profess. Pap. 1360,* 347–374.

Corbett, E. J. (1984). Seismicity and crustal structure studies of Southern California: tectonic implications from improved earthquake locations, *Ph.D. Thesis,* California Institute of Technology, Pasadena, California, 231 p.

Corbett, E. J., and C. E. Johnson (1982). The Santa Barbara, California, earthquake of 13 August 1978, *Bull. Seism. Soc. Am.* **72,** 2201–2226.

Crouch, J. K. (1981). Northwest margin of California continental borderland: marine geology and tectonic evolution, *Am. Assn. Petr. Geol.* **65,** 191–218.

Crouch, J. K., and J. Suppe (1993). Late Cenozoic tectonic evolution of the Los Angeles basin and inner California borderland: A model for core complex-like crustal extension, *Geol. Soc. Am. Bull.* **105,** 1415–1434.

Cruces F. J., and C. J. Rebollar (1991). Source parameters of the 22 December 1964 (m_b = 5.4, M_S = 6.2) offshore Ensenada earthquake, *Phys. Earth Planet. Int.* **66,** 253–258.

Dodge, D. A., G. C. Beroza, and W. L. Ellsworth (1996). Detailed observations of California foreshock sequences: implications for the earthquake initiation process, *J. Geophys. Res.* **101,** 22,371–22,392.

Evernden, J. F. (1969). Precision of epicenters obtained by small numbers of world-wiede stations, *Bull. Seism. Soc. Am.* **59,** 1365–1398.

Feigl, K. L., D. C. Agnew, Y. Bock, D. Dong, A. Donnellan, B. H. Hager, T. A. Herring, D. D. Jackson, T. H. Jordan, R. W. King, S. Larsen, K. M. Larson, M. H. Murray, Z. Shen, and F. H. Webb (1993). Space geodetic measurement of crustal deformation in central and southern California, 1984–1992, *J. Geophys. Res.* **98,** 21,677–21,712.

Fremont, M.-J., and S. D. Malone (1987). High precision relative locations of earthquakes at Mount St. Helens, *J. Geophys. Res.* **92,** 10,223–10,236.

Frohlich, C. (1979). An efficient method for joint hypocenter determination for large groups of earthquakes, *Comput. Geosci.* **5,** 387–389.

Gillard, D., A. M. Rubin, and P. Okubo (1996). Highly concentrated seismicity caused by deformation of Kilauea's deep magma system, *Nature* **384,** 343–346.

Got, J.-L., J. Frechet, and F. W. Klein (1994). Deep fault geometry inferred from multiplet relative relocation beneath the south flank of Kilauea, *J. Geophys. Res.* **99,** 15,375–15,386.

Gutenberg, B., C. F. Richter, and H. O. Woods (1932). The earthquake in Santa Monica Bay, California, on August 30, 1930, *Bull. Seism. Soc. Am.* **22,** 138–154.

Haase, J. S., P. M. Shearer, and R. C. Aster (1995). Constraints on temporal variations in velocity near Anza, California, from analysis of similar event pairs, *Bull. Seism. Soc. Am.* **85,** 194–206.

Hadley, D. M., and H. Kanamori (1977). Seismic structure of the Transverse Ranges, California, *Geol. Soc. Am. Bull.* **88,** 1469–1478.

Hauksson, E. (1987). Seismotectonics of the Newport-Inglewood fault zone in the Los Angeles basin, Southern California, *Bull. Seism. Soc. Am.* **77,** 539–561.

Hauksson, E. (1990). Earthquakes, faulting, and stress in the Los Angeles basin, *J. Geophys. Res.* **95,** 15,365–15,394.

Hauksson, E., and L. M. Jones (1988). The July 1986 Oceanside (M_L = 5.3) earthquake sequence in the Continental Borderland, Southern California, *Bull. Seism. Soc. Am.* **78,** 1885–1906.

Hauksson, E., and G. V. Saldivar (1986). The 1930 Santa Monica and the 1979 Malibu, California, earthquakes, *Bull. Seism. Soc. Am.* **76,** 1542–1559.

Hauksson, E., and G. V. Saldivar (1989). Seismicity and active compressional tectonics in Santa Monica Bay, Southern California, *J. Geophys. Res.* 94, 9,591–9,606.

Heaton, T. H., and L. M. Jones (1989). Seismological Research Issues in the San Diego Region, in G. Roquemore and S. Tanges (Editors), Workshop on "The Seismic Risk in the San Diego Region: Special Focus on the Rose Canyon Fault System," 29–30 June 1989, San Diego, California, 42–49.

Hey, R. N. (1998). Speculative propagating rift-subduction zone interactions with possible consequences for continental margin evolution, *Geol.* **26,** 247–250.

Howell, D. G., and J. Vedder (1981). Structural implications of stratigraphic discontinuities across the southern California Borderland, in *The Geotectonic Development of California,* Vol. 1, W. G. Ernst (Editor), Prentice-Hall, Englewood Cliffs, New Jersey.

Hutton, L. K., L. M. Jones, E. Hauksson, and D. D. Given (1991). Seismotectonics of southern California, in D. B. Slemmons, E. R. Engdahl, M. D. Zoback, and D. D. Blackwell (Editors), *Neotectonics of North America: Boulder, Colorado,* Geol. Soc. Am., Decade Map Volume 1.

Jennings, C. W. (1994). Fault activity map of California and adjacent areas. Geologic data map No. 6: faults, locations of recent volcanic eruptions, scale 1:750,000. California Division of Mines and Geology.

Jordan, T. H., and K. A. Sverdrup (1981). Teleseismic location techniques and their application to earthquake clusters in the south-central Pacific, *Bull. Seism. Soc. Am.* **71,** 1105–1130.

Junger, A. (1979). Tectonics of the Southern California Borderland, in *Aspects of the Geologic History of California Continental Borderland,* D. G. Howell (Editor), *Am. Assoc. Petr. Geol. Spec. Pub. 24,* 486–498.

Kanamori, H., and D. L. Anderson (1975). Theoretical basis of some empirical relations in seismology, *Bull. Seism. Soc. Am.* **65,** 1073–1095.

Kennedy, M. P., H. G. Greene, and S. H. Clarke (1987). Geology of the California continental margin: explanation of the California Continental Margin geologic map series, *Calif. Div. Mines Geol. Bull. 207.*

Larson, K. M. (1993). Application of the global positioning system to crustal deformation measurements. 3. Results from the Southern California Borderlands, *J. Geophys. Res.,* **98,** 21,713–21,726.

Lee, W. H. K., R. F. Yerkes, and M. Simirenko (1979). Recent earthquake activity and focal mechanisms in the western Transverse Ranges, California, *U.S. Geol. Surv. Circular 799,* 1–26.

Leeds, A. L. (1979). Relocation of M ≥ 5.0 northern Baja California earthquakes using *S-P* times, *Master Thesis,* University of California, San Diego.

Legg, M. R. (1991). Developments in understanding the tectonic evolution of the California Continental Borderland, in From shore-line to abyss. Contributions in marine geology in honor of Francis Parker Shepard, R. H. Osborne (Editor), *Soc. Sed. Geol. Spec. Pub. 46,* 291–312.

Legg, M. R. (1989). Faulting and seismotectonics of the inner continental Borderland west of San Diego, in G. Roquemore and S. Tanges (Editors), Worshop on "The Seismic Risk in the San Diego Region: Special Focus on the Rose Canyon Fault System," 29–30 June 1989, San Diego, California, 50–70.

Legg, M. R. (1985). Geologic structure and tectonics of the inner continental borderland offshore northern Baja California, Mexico, *Ph.D. Thesis,* University of California, Santa Barbara, 410 p.

Legg, M. R. (1980). Seismicity and tectonics of the Inner Continental Borderland of Southern California and Northern Baja California, Mexico, *Master's Thesis,* University of California, San Diego, 60 p.

Legg M. R., and M. P. Kennedy (1979). Faulting offshore San Diego and northern Baja California, in P. L. Abbot and W. J. Elliot, (Editors), *Earthquakes and other perils—San Diego Region, Geological Society of America Annual Meeting Guidebook,* 29–46.

Legg, M. R., and V. W. Ortega (1978). New evidence for major faulting in the inner borderland off northern Baja California, Mexico (abstract), *Trans. Am. Geophys. Union,* **59,** 1134.

Londsdale, P. (1991). Structural patterns of the Pacific floor offshore of Peninsular California, in *Gulf and peninsula province of the Californias,* J. P. Dauphine and B. T. Simoneit, (Editors), *Am. Assoc. Pet. Geol. Mem. 47,* 87–125.

Magistrale, H. (1993). Seismicity of the Rose Canyon Fault Zone near San Diego, California, *Bull. Seism. Soc. Am.* **83,** 1971–1978.

Magistrale, H., H. Kanamori, and C. Jones (1992). Forward and inverse three-dimensional P wave velocity models of the southern California crust, *J. Geophys. Res.* **97,** 14,115–14,135.

Mann, P., and M. B. Gordon (1996). Tectonic uplift and exhumation of blueschist belts along transpressional strike-slip fault zones, in *Subduction Top to Bottom,* G. E. Bebout, D. W. Scholl, S. H. Kirby, and J. P. Platt (Editors), American Geophysical Union, Washington, D.C., 143–154.

Mezcua, J., and J. Rueda (1994). Earthquake relative location based on waveform similarity, *Tectonophysics* **233,** 253–263.

Moore, D. G. (1969). Reflection profiling studies of the California Continental Borderland, *Geol. Soc. Am. Spec. Pap. 107,* 138 pp.

Mount V. S., and J. Suppe (1987). State of stress near the San Andreas fault: implications for wrench tectonics, *Geology* **15,** 1143–1146.

Nadeau, R. M., W. Foxall, and T. V. McEvilly (1995). Clustering and periodic recurrence of micoearthquakes on the San Andreas Fault at Parkfield, California, *Science* **267,** 503–507.

National Ocean Survey (1975). Bathymetric map, scale 1:250,000. Sheets 1206N-15 and 1206N-16.

Pacheco, J., and J. Nábêlek (1988). Source mechanisms of three moderate California earthquakes of July 1986, *Bull. Seism. Soc. Am.* **78,** 1907–1929.

Pechmann J. C., and B. S. Thorbjarnrdottir (1990). Waveform analysis of two preshock-main shock–aftershock sequences in Utah, *Bull. Seism. Soc. Am.* **80,** 519–551.

Pechmann, J. C., and H. Kanamori (1982). Waveforms and spectra of preshocks and aftershocks of the 1979 Imperial Valley, CA. earthquake: a test of the asperity model, *J. Geophys. Res.* **87,** 10,579–10,597.

Poupinet, G., W. L. Ellsworth, and J. Frechet (1984). Monitoring velocity variations in the crust using earthquake doublets: an application to the Calaveras Fault, California, *J. Geophys. Res.* **89,** 5719–5731.

Pujol, J. (1988). Comments on the joint determination of hypocenters and stations corrections, *Bull. Seism. Soc. Am.* **78,** 1179–1189.

Pujol, J. (1995). Application of the JHD technique to the Loma Prieta, California, mainshock–aftershock sequence and implications for earthquake location, *Bull. Seism. Soc. Am.* **85,** 129–150.

Richter, C. F. (1958). *Elementary Seismology*, W. H. Freeman, San Francisco, 768 p.

Rubin, A. M., D. Gillard, and J.-L. Got (1999). Streaks of microearthquakes along creeping faults, *Nature* **400,** 635–641.

Saldivar, G. V. (1987). Seismotectonics of the Santa Monica and Palos Verdes fault systems in the Santa Monica Bay, southern California, *Master's thesis*, University of Southern California, Los Angeles, 90 pp.

Sambridge, M., J. Braun, and H. McQueen (1995). Geophysical parametrization and interpolation of irregular data using natural neighbors, *Geophys. J. Int.* **122,** 837–857.

Shearer, P. (1997). Improving local earthquake locations using the L1 norm and waveform cross correlation: application to the Whittier Narrows, California, aftershock sequence, *J. Geophys. Res.* **102,** 8269–8283.

Shearer, P. (1998). Evidence from a cluster of small earthquakes for a fault at 18 km depth beneath Oak Ridge, southern California, *Bull. Seism. Soc. Am.* **88,** 1327–1336.

Shor, G. G., R. W. Raitt, and D. D. McGowan (1976). Seismic refraction studies in the southern California Borderland, *Marine Physics Laboratory, Scripps Institution of Oceanography, Report 76-13,* 70 pp.

Slad, G. W., and R. C. Aster (1995). Microearthquake relocation implementing similar event analysis in the hypocentral regions of southern California mainshocks, *Seism. Res. Lett.* **66,** 45–49.

Stierman D. J., and W. L. Ellsworth (1976). Aftershocks of the February 21, 1973 Point Mugu, California earthquake, *Bull. Seism. Soc. Am.* **66,** 1931–1952.

Sylvester, A. G., S. W. Smith, and C. H. Scholtz (1970). Earthquake swarm in the Santa Barbara Channel, California, 1968, *Bull. Seism. Soc. Am.* **60,** 1047–1060.

Vedder, J. G., L. A. Beyere, A. Junger, G. W. Moore, A. E. Robets, J. C. Taylor, and H. C. Wagner (1974). Preliminary report on the geology of the continental borderland of southern California, *U.S. Geol. Surv. Misc. Field Studies 624.*

Weldon R., and E. Humphreys (1986). A kinematic model of southern California, *Tectonics* **5,** 33–48.

Wessel, P., and H. F. Smith (1991). Free software helps map and display data, *EOS Trans. AGU,* **72,** 441, 445–446.

Woodward-Clyde Consultants (1979). Report on the evaluation of maximum earthquake and site ground motion parameters associated with the Offshore Zone of Deformation, San Onofre Nuclear Generation Station, Los Angeles, California: Report prepared for Southern California Edison, 56 p.

Whitcomb, J. H., *et al.* (1979). Caltech-U.S. Geological Survey monthly preliminary epicenters from March 1978 to January 1979, Seismo-Lab. Report, California Institute of Technology, Pasadena, California.

Yeats, R. S. (1976). Extension vs. strike-slip origin of the southern California continental borderland, in D. G. Howell (Editor), *Aspects of the Geologic History of California Continental Borderland, Am. Assoc. Petr. Geol. Spec. Pub. 24,* 455–485.

Zoback, M. D., M. L. Zoback, V. S. Mount, J. Suppe, J. P. Eaton, J. H. Healy, D. Oppenheimer, P. Reasenberg, L. Jones, C. B. Raleigh, I. G. Wong, O. Scotti, and C. Wentworth (1987). New evidence on the state of stress of the San Andreas fault system, *Science* **238,** 1105–1111.

Institute of Geophysics and Planetary Physics
Scripps Institution of Oceanography
University of California, San Diego
La Jolla, California 92093-0225

Manuscript received 12 February 1999.